

NSUSY fits

José R. Espinosa,¹ Christophe Grojean,² Verónica Sanz,^{2,3} and Michael Trott²

¹*ICREA at IFAE, Universitat Autònoma de Barcelona, 08193 Bellaterra, Barcelona, Spain*

²*Theory Division, Physics Department, CERN, CH-1211 Geneva 23, Switzerland*

³*Department of Physics and Astronomy, York University, Toronto, ON, Canada, M3J 1P3*

(Dated: August 1, 2012)

We perform a global fit to Higgs signal-strength data in the context of light stops in Natural SUSY. In this case, the Wilson coefficients of the higher dimensional operators mediating $g g \rightarrow h$ and $h \rightarrow \gamma \gamma$, given by c_g, c_γ , are related by $c_g = 3(1 + 3\alpha_s/(2\pi))c_\gamma/8$. We examine this predictive scenario in detail, combining Higgs signal-strength constraints with recent precision measurements of m_W , $\text{Br}(\bar{B} \rightarrow X_s \gamma)$ constraints and direct collider bounds on weak scale SUSY, finding regions of parameter space that are consistent with all of these constraints. However it is challenging for the allowed parameter space to reproduce the observed Higgs mass value with sub-TeV stops. We discuss some of the direct stop discovery prospects and show how Higgs search data can be used to exclude light stop parameter space difficult to probe by direct collider searches. We determine the current status of such indirect exclusions and estimate their reach by the end of the 8 TeV LHC run.

I. INTRODUCTION

The discovery of the Standard Model (SM) Higgs (assuming that the discovered boson is the SM Higgs) puts Supersymmetry (SUSY) to a new test. The possibility that SUSY solves the hierarchy problem without re-introducing fine-tuning i.e. the paradigm of Natural SUSY (NSUSY) [1–7] can now be examined in the light of increasingly precise measurements of the properties of the Higgs.

NSUSY predicts new particles near the electroweak (EW) scale, which necessarily must affect the properties of the Higgs if they are to stabilize this scale. The minimalistic scenario for NSUSY focuses on the vestige of the SUSY spectrum which is required to be light in order to keep the fine-tuning of the theory reasonably small. In this case, the most significant impact of new states on Higgs phenomenology is through the presence of light stop states. This scenario is not just

motivated by simplicity, but also by the lack of evidence for SUSY to date, indicating that a weak scale SUSY spectrum needs to be non-generic to satisfy collider constraints. The states directly related to naturalness (primarily the stop and Higgsinos) are especially challenging, and model independent collider bounds are weak or non-existent.

Conversely, the study of the impact of an NSUSY scenario on the properties of the Higgs benefits from the enormous effort expended by the experimental collaborations in refining the accuracy and precision of the reported Higgs signal strength measurements. When considering the experimentally resolvable impact of NSUSY, indirect probes, *e.g.* through a fit to Higgs properties, electroweak precision data and flavor physics may well be more powerful in constraining many minimal scenarios than direct searches for some time. This is the line of reasoning we develop in this paper, where we examine the current constraints on minimal NSUSY from these indirect probes.

The outline of this paper is as follows. We briefly review and introduce NSUSY in Section II. In Section III we then review the impact of the NSUSY spectra on the properties of the SM Higgs through modifications in the loop-induced $h \rightarrow g g$ and $h \rightarrow \gamma \gamma$ couplings. Further, in Section IV we work through the constraints set on NSUSY from global fits to Higgs properties in the presence of light stops. We advance such studies by using a more complete global fit (now including 48 signal strength channels, including ICHEP and post ICHEP data updates)¹. We make use of the fixed relationship between the Wilson coefficients (including the QCD matching corrections) for $h\gamma\gamma$ and hgg in the case of NSUSY to perform a one-parameter fit and then directly map the allowed parameter space in global Higgs fits into the allowed stop space. Further, we determine 95% confidence level (C.L.) exclusion limits on the stop parameter space derived from Higgs search data. We then consider constraints from $\text{BR}(\bar{B} \rightarrow X_s \gamma)$ and recent precision measurements of m_W at the Tevatron, as these results, which are under excellent theoretical control, are sensitive to light stops. The (statistically insignificant, but interesting) deviations from the SM predictions in these observables in a weak scale NSUSY scenario could offer some further resolution on the allowed stop parameter space, if NSUSY exists. Ascribing these deviations to the effect of stops in NSUSY, such stop states are consistent with the results of the global fits to Higgs signal strengths, as we will show. Finally, we also take into account direct collider bounds. In Section V we discuss

¹ Some past papers that have consistently examined earlier versions of the Higgs dataset in this context, with varying degrees of sophistication, are [8–17].

Field	Spin	$SU(3)_c \times SU(2)_L \times U(1)_Y$
$\tilde{Q}_L = (\tilde{t}_L, \tilde{b}_L)$	0	$(\mathbf{3}, \mathbf{2}, 1/6)$
\tilde{t}_R^*	0	$(\bar{\mathbf{3}}, \mathbf{1}, -2/3)$
$H_u = (H_u^+, H_u^0)$	0	$(\mathbf{1}, \mathbf{2}, +1/2)$
$H_d = (H_d^0, H_d^-)$	0	$(\mathbf{1}, \mathbf{2}, -1/2)$
$\tilde{H}_u = (\tilde{H}_u^+, \tilde{H}_u^0)$	1/2	$(\mathbf{1}, \mathbf{2}, +1/2)$
$\tilde{H}_d = (\tilde{H}_d^0, \tilde{H}_d^-)$	1/2	$(\mathbf{1}, \mathbf{2}, -1/2)$
\tilde{g}	1/2	$(\mathbf{8}, \mathbf{1}, 0)$

TABLE I: *The minimal NSUSY field content. In our analysis, gluinos and a heavy linear combination of the Higgs doublets will be further integrated out.*

the interplay of these constraints and determine the allowed parameter space that remains. We include the limits coming from the Higgs mass measurement and estimate the degree of fine-tuning incurred, finding that some regions of the stop parameter space that give a reasonable global fit also allow the Higgs mass to be raised to its observed value. In Section VI we discuss the current exclusion bounds that can be derived using these indirect probes of stop parameter space. To study the future prospects of such limits by the end of 2012, assuming that the experimental error in Higgs signal-strength measurements scales down as $\sim 1/\sqrt{\mathcal{L}_{int}}$, we consider two hypothetical cases: 1) the current pattern of best-fit signal-strength values does not change, and 2) the dataset evolves to converge on the SM expected signal strengths. Finally, in Section VII we conclude.

II. NATURAL SUSY

Naively, in generic SUSY scenarios motivated as a solution to the hierarchy problem, one expects all superpartners near the electroweak scale, with the soft breaking mass scale M_{SUSY} not higher than $\mathcal{O}(1)$ TeV. The experimental picture emerging from the LHC is in growing tension with this expectation. After searching in many typical discovery channels, and reaching a peak sensitivity of roughly $\mathcal{O}(1.5\text{TeV})/\mathcal{O}(100)$'s GeV, for coloured/electroweak SUSY states [18], no statistically significant experimental excess has been reported to date. On the other hand, to avoid destabilizing the electroweak scale when $M_{\text{SUSY}} \gg v$ (without fine-tuning), only a minimal set of SUSY particles have to be light ($\lesssim 1 - 2$ TeV) [1–7]. The stop soft masses are directly connected (at one-loop) to the Higgs mass scale (or Z mass) through the sizable top coupling, so fine-tuning

considerations require them to be light. Although sbottoms (\tilde{b}) do not directly affect the fine-tuning of the Z mass, \tilde{b}_L is required to be light as it is linked to the \tilde{t}_L mass scale by $SU(2)_L$ symmetry. The Higgsino mass coming from the μ term² is tied to tree-level contributions to the Higgs mass. With gaugino masses assumed heavy, of order M_{SUSY} , light charginos and neutralinos are almost pure Higgsinos, with mass given by μ up to corrections of order v/M_{SUSY} that we neglect. To a lesser degree, the gluinos \tilde{g} are also expected to be light due to their contribution to two-loop corrections to the Higgs mass parameter, which leads to the rough estimate $m_{\tilde{g}} \lesssim 2m_{\tilde{t}} (4m_{\tilde{t}})$ for a Majorana (Dirac) gluino [6]. In practice, we can also decouple these somewhat heavier gluinos in our analysis.

The states just discussed are listed in Table I. These are the states whose impact on Higgs signal strengths and low-energy precision measurements we will focus on in this paper. We will not consider light staus ($\tilde{\tau}^\pm$), which can also modify the Higgs decays to photons, see Refs. [8, 9] for recent studies. We neglect these states as we assume a moderate value of $\tan \beta \lesssim \mathcal{O}(10)$, for which $\tilde{\tau}^\pm$ effects are negligible compared to the stop contribution. We also neglect the effects of the \tilde{b} on the Higgs mass and in the loop corrections to the Higgs signal strength parameters for the same reason.

Regarding the SUSY Higgs sector, we will consider the decoupling regime in which only one Higgs doublet remains light³, while the second doublet, with mass controlled by the pseudoscalar mass m_A , has a mass $\sim \text{TeV}$. In this limit, the couplings of the lightest Higgs h to fermions and gauge bosons approach their SM values, and we will only consider deviations in the loop-induced couplings of the light h to photons and gluons (see next section).

In order to fix our notation, we write now the parts of the low-energy Lagrangian most relevant for our analysis. This Lagrangian is not supersymmetric as it applies below the scale of the heavy SUSY particles (with masses $\sim M_{SUSY} \gtrsim 1 \text{ TeV}$). Supersymmetric relations between some couplings are broken and one should introduce different couplings, to be matched to the supersymmetric theory at the scale M_{SUSY} . In practice, the hierarchy between M_{SUSY} and the electroweak scale is mild and one can neglect most of these breaking effects. One important exception is the

² In this paper we distinguish signal-strengths with a subscript, μ_i for a final state i , from the μ parameter in NSUSY, which carries no subscript.

³ This choice is supported by the results of Ref. [17], where the 2HDM is studied in the light of the Post-Moriond Higgs data and no compelling region in the parameter space of the MSSM consistent with the data was identified, except the decoupling limit.

Higgs quartic coupling, as will be discussed later on.

From the superpotential $W = \mu H_d \cdot H_u + h_t Q_L \cdot H_u t_R^c$, the Lagrangian gets the terms

$$\delta\mathcal{L} = \mu \tilde{H}_d \cdot \tilde{H}_u + h_t Q_L \cdot H_u t_R^c + h_t \tilde{Q}_L \cdot \tilde{H}_u t_R^c + h_t Q_L \cdot \tilde{H}_u \tilde{t}_R^* + \text{h.c.} \quad (1)$$

where \cdot stands for the $\text{SU}(2)_L$ product: $H_d \cdot H_u = H_d^0 H_u^0 - H_d^- H_u^+$ and we have suppressed $\text{SU}(3)$ indices for (s)quarks. (Weyl) fermionic fields are contracted in the usual way: $\tilde{H}_d^0 \tilde{H}_u^0 = i(\tilde{H}_d^0)^T \sigma_2 \tilde{H}_u^0$. Eq. (1) contains a Dirac mass term μ for Higgsinos, the top Yukawa coupling between top quarks and the Higgs, and the related Higgsino-squark-quark couplings, relevant for the contribution of Higgsino-stops to $\text{Br}(\bar{B} \rightarrow X_s \gamma)$.

The scalar potential for Higgses and squarks is well known and includes supersymmetric F and D terms and soft-SUSY-breaking terms. We can always perform a rotation of the full Higgs doublets $H_{u,d}$ to the doublets $H_{l,h}$:

$$\begin{pmatrix} H_l \\ \bar{H}_h \end{pmatrix} = \begin{pmatrix} \cos \beta & \sin \beta \\ -\sin \beta & \cos \beta \end{pmatrix} \begin{pmatrix} \bar{H}_d \\ H_u \end{pmatrix}, \quad (2)$$

where $\tan \beta \equiv \langle H_u^0 \rangle / \langle H_d^0 \rangle = v_u / v_d$ and \bar{H}_d denotes the $\text{SU}(2)$ conjugate, $\bar{H}_d = -i\sigma^2 H_d^* = (-H_d^+, H_d^{0*})$, in such a way that H_l is the doublet involved in electroweak symmetry breaking while H_h does not take a vacuum expectation value. In the Higgs decoupling limit, with large pseudoscalar mass, H_h is in fact composed of the heavy fields H^0, A^0, H^\pm , while H_l is SM-like and contains the light Higgs h and the Goldstones. The quartic H_l coupling determines the light Higgs mass as usual and is the prime example of a coupling that receives sizeable SUSY-breaking corrections (that help in increasing the Higgs mass above its tree level minimal SUSY value below m_Z). Such corrections will be discussed in Subsection V.A.

Finally, the stop masses are given by the mass matrix

$$\mathcal{M}_{\tilde{t}}^2 = \begin{bmatrix} M_{LL}^2 & M_{LR}^2 \\ M_{RL}^2 & M_{RR}^2 \end{bmatrix} = \begin{bmatrix} M_{\tilde{Q}_L}^2 + m_t^2 + m_Z^2 \left(\frac{1}{2} - \frac{2}{3} s_w^2 \right) c_{2\beta} & m_t (A_t + \mu / \tan \beta) \\ m_t (A_t + \mu / \tan \beta) & M_{\tilde{t}_R}^2 + m_t^2 + \frac{2}{3} m_Z^2 s_w^2 c_{2\beta} \end{bmatrix}, \quad (3)$$

where we used $c_{2\beta} = \cos 2\beta$, m_t is the top mass and $M_{\tilde{Q}_L}, M_{\tilde{t}_R}, A_t$ are soft SUSY-breaking masses. The stop mixing angle θ_t relates the interaction eigenstates $\tilde{t}_{L,R}$ to the mass eigenstates $\tilde{t}_{1,2}$ by the rotation

$$\begin{pmatrix} \tilde{t}_1 \\ \tilde{t}_2 \end{pmatrix} = \begin{pmatrix} \cos \theta_t & -\sin \theta_t \\ \sin \theta_t & \cos \theta_t \end{pmatrix} \begin{pmatrix} \tilde{t}_L \\ \tilde{t}_R \end{pmatrix}. \quad (4)$$

The mixing angle $\theta_{\tilde{t}}$ is taken in the interval $(-\pi/2, \pi/2)$ and defined by

$$\cos 2\theta_{\tilde{t}} \equiv \frac{M_{RR}^2 - M_{LL}^2}{\sqrt{(M_{LL}^2 - M_{RR}^2)^2 + 4M_{LR}^4}}, \quad \sin 2\theta_{\tilde{t}} \equiv \frac{2M_{LR}^2}{\sqrt{(M_{LL}^2 - M_{RR}^2)^2 + 4M_{LR}^4}}, \quad (5)$$

with the signs of $M_{RR}^2 - M_{LL}^2$ and M_{LR}^2 determining the quadrant of $2\theta_{\tilde{t}}$. With this definition of $\theta_{\tilde{t}}$, one automatically guarantees $m_{\tilde{t}_1} \leq m_{\tilde{t}_2}$, with

$$m_{\tilde{t}_2}^2 - m_{\tilde{t}_1}^2 \equiv (\delta m)^2 = \sqrt{(M_{LL}^2 - M_{RR}^2)^2 + 4M_{LR}^4}. \quad (6)$$

Finally, neglecting sbottom mixing (proportional to m_b), the light sbottom has mass $m_{\tilde{b}_L}^2 = M_{\tilde{Q}_L}^2 + m_b^2 - m_Z^2(1/2 - s_w^2/3) \cos 2\beta$, while the heavy \tilde{b}_R is decoupled.

III. LOOP-LEVEL CORRECTIONS TO HIGGS PROPERTIES IN NSUSY

In this section, we review the loop-level NSUSY corrections to the couplings of h to photons and gluons.⁴ The leading correction from stops to the gluon-fusion process is given by [19, 20]

$$\frac{\sigma(gg \rightarrow h)}{\sigma^{SM}(gg \rightarrow h)} \simeq \frac{\Gamma(h \rightarrow gg)}{\Gamma^{SM}(h \rightarrow gg)} \simeq |1 + r_g|^2, \quad (7)$$

where

$$r_g = \frac{C_g(\alpha_s) F_g(m_{\tilde{t}_1}, m_{\tilde{t}_2}, \theta_{\tilde{t}})}{F_g^{SM}(m_t, m_b \dots)}. \quad (8)$$

Here $C_g(\alpha_s)$ is a factor that takes into account higher order QCD corrections— see the discussion below— and the F_g functions are defined as follows

$$F_g(m_{\tilde{t}_1}, m_{\tilde{t}_2}, \theta_{\tilde{t}}) = \sum_{i=\tilde{t}_1, \tilde{t}_2, \dots} g_{hi} \frac{m_Z^2}{m_i^2} F_0(\tau_i), \quad (9)$$

$$F_g^{SM}(m_t, m_b \dots) = \sum_{i=t, b, \dots} F_{1/2}(\tau_i) \left(1 + \frac{11\alpha_s}{4\pi} \right) \approx -2/(1.41 + 0.14i), \quad (10)$$

where $\tau_i = m_h^2/(4m_i^2)$, $F_0(\tau) = [\tau - f(\tau)]/\tau^2$ and $F_{1/2}(\tau) = [\tau + (\tau - 1)f(\tau)]/\tau^2$ with $f(\tau) = \arcsin^2 \sqrt{\tau}$ for $\tau \leq 1$ while, for $\tau > 1$,

$$f(\tau) = -\frac{1}{4} \left[\log \frac{1 + \sqrt{1 - \tau^{-1}}}{1 - \sqrt{1 - \tau^{-1}}} - i\pi \right]^2. \quad (11)$$

⁴ The effects of NSUSY loop corrections on the decay $\Gamma(h \rightarrow Z\gamma)$ are neglected as the leading effects in these scenarios come from charged scalars in the loop, and we are considering the decoupling limit in the scalar sector (consistent with the minimal version of NSUSY).

See the Appendix for the SM inputs used in determining the numerical value of F_g^{SM} above.

The couplings $g_{h\tilde{t}_i\tilde{t}_i}$ are given, in the decoupling limit [21], by

$$g_{h\tilde{t}_i\tilde{t}_i} \frac{m_Z^2}{m_t^2} = -1 - \langle \tilde{t}_i | \tilde{t}_L \rangle \frac{M_{LR}^2}{4m_t^2} \langle \tilde{t}_R | \tilde{t}_i \rangle - \frac{m_Z^2 c_{2\beta}}{12m_t^2} [(3 - 4s_W^2) |\langle \tilde{t}_i | \tilde{t}_L \rangle|^2 + 4s_W^2 |\langle \tilde{t}_i | \tilde{t}_R \rangle|^2] , \quad (12)$$

where $M_{LR}^2 = m_t(A_t + \mu/\tan\beta) = (m_{\tilde{t}_2}^2 - m_{\tilde{t}_1}^2) \sin\theta_{\tilde{t}} \cos\theta_{\tilde{t}}$ has been defined in Eq. (3); the $\langle \tilde{t}_i | \tilde{t}_{L,R} \rangle$ can be directly read from Eq. (4); and we have included the D -term contributions proportional to $\cos 2\beta$, although their effect is negligible. The sign of $\sum_{i=1,2} g_{h\tilde{t}_i\tilde{t}_i} \tau_i$ is negative if the the stop sector is dominated by a light eigenstate of pure chirality, and positive if the term in M_{LR}^2 dominates, $M_{LR}^4 \gtrsim 4m_t^2(m_{\tilde{t}_1}^2 + m_{\tilde{t}_2}^2)$. In the no-mixing case, we expect a reduction of $\sigma(gg \rightarrow h)$. In the maximal-mixing case, the enhancement depends on the separation between the two eigenstates.

The decay width $\Gamma(h \rightarrow \gamma\gamma)$ is also modified by stop loops through the same function in Eq. (10), as the non-Abelian nature of QCD is irrelevant for the leading-order loop function. One finds [19] the correction

$$\frac{\Gamma(h \rightarrow \gamma\gamma)}{\Gamma^{SM}(h \rightarrow \gamma\gamma)} \simeq |1 + r_\gamma|^2, \quad r_\gamma = \frac{N_c Q_{\tilde{t}}^2 C_\gamma(\alpha_s) F_g(m_{\tilde{t}_1}, m_{\tilde{t}_2}, \theta_{\tilde{t}})}{F_\gamma^{SM}(m_t, W, m_b \dots)}. \quad (13)$$

The SM contribution is given by

$$F_\gamma^{SM}(m_t, W, m_b \dots) = F_1(\tau_W) + \sum_{i=t,b,\dots} N_c Q_i^2 F_{1/2}(\tau_i) \left(1 - \frac{\alpha_s}{\pi}\right) \approx 1/(0.155 - 0.002i), \quad (14)$$

where $F_1(\tau) = [2\tau^2 + 3\tau + 3(2\tau - 1)f(\tau)]/\tau^2$, N_c is the number of colours, and Q_i is the electric charge with e factored out. The matching correction in this case is given by $C_\gamma(\alpha_s)$, to be further discussed in the next section.

In the no-mixing limit, the effect of the stop is to increase the branching ratio to photons. When the mixing term in Eq.(12) dominates, the effect is to reduce it. The total cross section $gg \rightarrow h \rightarrow \gamma\gamma$ accounts for those two opposite effects, but the combination tends to follow whatever is the sign of the gluon fusion modification.

IV. CURRENT CONSTRAINTS ON NSUSY

A. Effective Theory Approach

It is useful to consider the approximation that all of the light NSUSY states are still heavy enough to be integrated out giving local operators. We can then fit to the data directly using the

effective Lagrangian⁵

$$\begin{aligned}\mathcal{L}_{HD} = & -\frac{c_g g_3^2}{2\Lambda^2} H^\dagger H G_{\mu\nu}^A G^{A\mu\nu} - \frac{c_W g_2^2}{2\Lambda^2} H^\dagger H W_{\mu\nu}^a W^{a\mu\nu} - \frac{c_B g_1^2}{2\Lambda^2} H^\dagger H B_{\mu\nu} B^{\mu\nu}, \\ & -\frac{c_{WB} g_1 g_2}{2\Lambda^2} H^\dagger \tau^a H B_{\mu\nu} W^{a\mu\nu},\end{aligned}\quad (15)$$

where g_1, g_2, g_3 are the weak hypercharge, SU(2) gauge and SU(3) gauge couplings and the scale Λ corresponds to the mass of the NSUSY states integrated out. The effects in NSUSY appear at the loop level, so we find it convenient to rescale the Wilson coefficients as $c_j = \tilde{c}_j/(16\pi^2)$. In this case, using the results of Ref. [22], the effect of the operators in (15) is

$$\sigma_{gg\rightarrow h} \approx \sigma_{gg\rightarrow h}^{SM} \left| 1 + \frac{2}{F_g^{SM}} \frac{v^2 \tilde{c}_g}{\Lambda^2} \right|^2, \quad \Gamma_{h\rightarrow\gamma\gamma} \approx \Gamma_{h\rightarrow\gamma\gamma}^{SM} \left| 1 + \frac{1}{F_\gamma^{SM}} \frac{v^2 \tilde{c}_\gamma}{\Lambda^2} \right|^2. \quad (16)$$

Here $\tilde{c}_\gamma = \tilde{c}_W + \tilde{c}_B - \tilde{c}_{WB}$. We can translate the effect of stops in the language of local operators by inspecting our expressions in Sec. III and those in Eq. (16),

$$\frac{v^2 \tilde{c}_g}{\Lambda^2} \simeq C_g(\alpha_s) \frac{F_g}{2}, \quad \frac{v^2 \tilde{c}_\gamma}{\Lambda^2} \simeq N_c Q_t^2 C_\gamma(\alpha_s) F_g. \quad (17)$$

These relationships are only approximate in the sense that the limit $m_{\tilde{t}_{1,2}} \gg m_h$ should be taken in the loop functions r_g, r_γ to match onto the local operators. If the two stop mass eigenstates can be integrated out simultaneously, the matching can be directly performed by expanding the loop functions in this limit, and one obtains⁶

$$F_g = \frac{1}{3} \left[\frac{m_t^2}{m_{\tilde{t}_1}^2} + \frac{m_t^2}{m_{\tilde{t}_2}^2} - \frac{1}{4} \sin^2(2\theta_t) \frac{\delta m^4}{m_{\tilde{t}_1}^2 m_{\tilde{t}_2}^2} \right]. \quad (18)$$

While, in this limit, the QCD matching corrections take the simple form

$$C_g(\alpha_s) = 1 + \frac{25\alpha_s}{6\pi}, \quad C_\gamma(\alpha_s) = 1 + \frac{8\alpha_s}{3\pi}. \quad (19)$$

These perturbative corrections are the matching corrections due to top squarks in the loops that do not cancel when a ratio is taken with the SM contribution to these loops. This correction factor

⁵ We do not include CP violating operators, assuming that all non-SM CP violating phases of the states integrated out are negligible. It has been argued [6] that this can be naturally accomplished in NSUSY when additional assumptions are employed concerning R-parity for example. Our assumption is conservative as the existence of large CP violating phases would only increase the constraints on an NSUSY spectrum.

⁶ Here we have neglected D term contributions, although we retain the effect of D terms in some of the numerical results presented. These corrections are negligible except for $m_{\tilde{t}_1} < 150$ GeV masses. They introduce a (minor) $\tan\beta$ dependence into the definition of F_g in the local operator approximation when retained.

is obtained in Ref. [23] in the limit where gluino effects and the effect of squark mixing was neglected.⁷ This approach also neglects running that would sum large logs if a two stage matching was employed, integrating out each stop eigenstate in sequence.⁸

Whether one integrates out the stops and matches onto the local operator approximation or not, there is a relationship between the NP effects on $\sigma_{gg \rightarrow h}$ and $\sigma_{h \rightarrow \gamma\gamma}$ that is independent of the stop mass parameters in the minimal NSUSY limit. In the local operator approximation, the relationship is simply

$$\frac{\tilde{c}_g}{\tilde{c}_\gamma} = \frac{1}{2N_c Q_t^2} \frac{C_g(\alpha_s)}{C_\gamma(\alpha_s)} = \frac{3}{8} \left(1 + \frac{3\alpha_s}{2\pi} \right), \quad (20)$$

where we see how the ratio $\sim 3/8$ is determined by the stop quantum numbers. This is a consequence of assuming that the only BSM contribution to both the $\gamma\gamma$ and gg loops comes from stops. This strong relationship will be relaxed in less minimal scenarios. For example, light χ^\pm 's with mass $m_{\chi_1^\pm}^2 \sim \mu^2$ (in the decoupling limit) would in principle also contribute to the $\gamma\gamma$ loops. However, the Higgs couples to the higgsino as $h \tilde{W}^\pm \tilde{H}^\mp$ and a large mixing between wino and higgsino eigenstates would be required. As we are considering the large gaugino mass limit in NSUSY, $M_2 \gg \mu, v$, this mixing scales as $\sim m_W^2 \sin^2 \beta / (M_2^2)$ and is suppressed, so that we can neglect the chargino contribution to $h\gamma\gamma$.

We also utilize this effective Lagrangian to examine the issue of efficiency corrections to the μ_i when high-dimension operators are present. We find that such efficiency corrections to event rates are very small and neglect them. See the Appendix for details.

B. Global Fit To Higgs Signal Strengths

In this section we describe our method and results for globally fitting to Higgs signal strength data in the scenario discussed above. Here we only briefly review the fit procedure, the details of our fit method are given in [26–28].⁹ Our fit incorporates the recently released 7 and 8 TeV LHC

⁷ It has been pointed out that $m_{\tilde{g}} \rightarrow \infty$ leads to mixed stop-gluino UV divergences [24] requiring extra counter-terms, but this technical requirement is not a barrier to the numerical investigations we perform. The full matching correction is given in Ref. [25]: the gluino contributions and stop mixing effects are a small correction to the $\sim 5\%$ matching correction we consider.

⁸ There are also perturbative corrections to the matrix element of the local effective operator $h G_{\mu\nu}^A G^{A\mu\nu}$. These are common multiplicative factors, as are soft gluon re-summation effects, and cancel in the ratios taken.

⁹ For other model-independent approaches to the determination of the Higgs couplings, see [10, 11, 29–35].

data [36–39], and the recently reported Tevatron Higgs results [40]. The data we use is listed in the Appendix. We fit to the available Higgs signal-strength data,

$$\mu_i = \frac{[\sum_j \epsilon_{ij} \sigma_{j \rightarrow h} \times \text{Br}(h \rightarrow i)]_{\text{observed}}}{[\sum_j \epsilon_{ij} \sigma_{j \rightarrow h} \times \text{Br}(h \rightarrow i)]_{SM}}, \quad (21)$$

for the production of a Higgs that decays into the observed channels $i = 1 \cdots N_{ch}$. Here N_{ch} denotes the number of channels, the label j in the cross section, $\sigma_{j \rightarrow h}$, is due to the fact that some final states are summed over different Higgs production processes, labelled with j . The ϵ_{ij} are the efficiency factors for the various production processes producing a final state j to pass experimental cuts. The reported best-fit value of a signal strength we denote by $\hat{\mu}_i$, and the χ^2 we construct is defined as

$$\chi^2(\mu_i) = \sum_{i=1}^{N_{ch}} \frac{(\mu_i - \hat{\mu}_i)^2}{\sigma_i^2}. \quad (22)$$

The covariance matrix has been taken to be diagonal with the square of the 1σ theory and experimental errors added in quadrature giving σ_i . We necessarily neglect correlation coefficients as these are not supplied. For the experimental errors we use \pm symmetric 1σ errors on the reported $\hat{\mu}_i$, while for theory predictions and related errors we use the results of the LHC Higgs Cross Section Working Group [41]. The minimum (χ_{min}^2) is determined, and the 68.2% (1σ), 95% (2σ), 99% (3σ) best fit regions are plotted as $\chi^2 = \chi_{min}^2 + \Delta\chi^2$, with the appropriate cumulative distribution function (CDF) defining the corresponding $\Delta\chi^2$.

We first perform a one-parameter fit in terms of the free parameter F_g , that depends on the stop sector of NSUSY, and plot $\chi^2 - \chi_{min}^2$ in Fig. 1 (left). This χ^2 distribution is directly related to the fit in the broader space of the generic Wilson coefficients of the local operators contributing to $h \rightarrow \gamma\gamma$ and $gg \rightarrow h$, as shown in Fig. 1 (right), although the match of the C.L. regions is only approximate due to the difference in number of degrees of freedom in the fit. It is not surprising that with the addition of this free parameter, the χ^2 measure is improved as compared to the SM. However, it was by no means guaranteed that the stop line determined by the NSUSY relationship between the Wilson coefficients would pierce the best fit region away from the SM one. This accidental fact allows a $\sim 2\sigma$ improvement of the fit. Although this is intriguing, we caution the reader that the interval of Wilson coefficients that intersect the 1σ best fit region is mapped into a very narrow range of stop mass parameters, corresponding to a tuned area of parameter space. In addition, best-fit regions in $(\tilde{c}_\gamma, \tilde{c}_g)$ space more distant from the SM point at $(0, 0)$ will generically

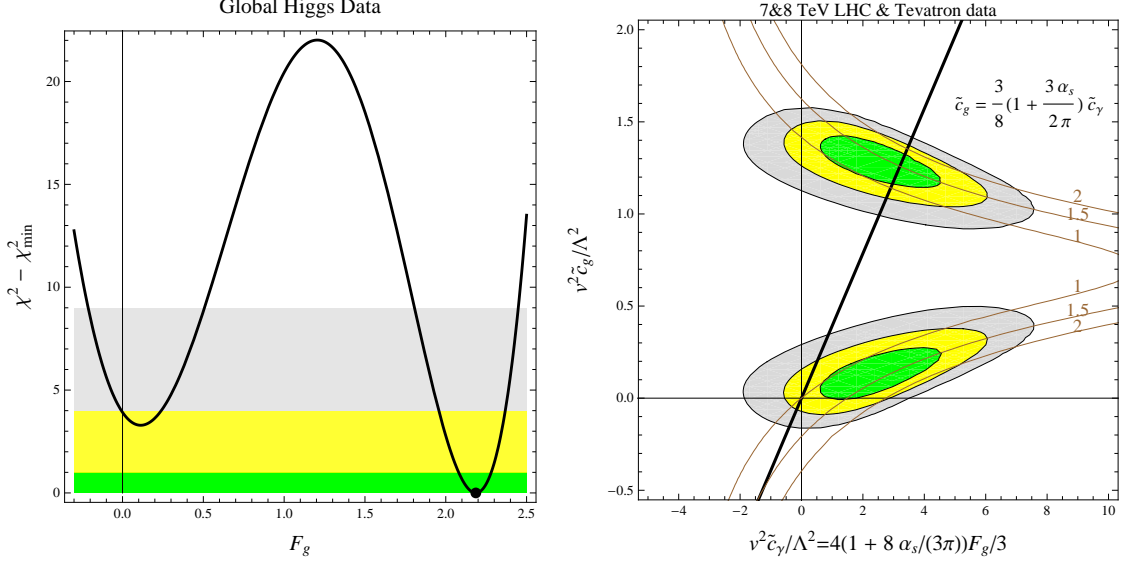


FIG. 1: The one dimensional fit to F_g in the NSUSY scenario to global Higgs data (left), and the approximate projection of the relationship between the Wilson coefficients into the higher dimensional operator space (right). The green, yellow and gray regions correspond to the 1, 2, 3 σ allowed regions in the 1D or 2D fit space (defined with the CDF appropriate to each case. This difference accounts for the mismatch in the $\Delta\chi^2$'s that define the best-fit regions). Also shown as solid (brown) contours is the enhancement of the $\mu_{\gamma\gamma}$ signal strength and how such a condition projects into the best fit space.

correspond to lighter states, as their impact scales as $1/\Lambda^2$. This will represent a further problem for this region.

We can characterize the allowed relationship between the Wilson coefficients that intersect the (1σ) best fit region in a model-independent way, finding that current data is consistent with the following four ranges of the Wilson coefficient ratios, corresponding to the four different best-fit regions in that 2D space [28].¹⁰ For $\tilde{c}_\gamma > 0$:

$$-0.01 < \tilde{c}_g/\tilde{c}_\gamma < 0.16, \quad 0.27 < \tilde{c}_g/\tilde{c}_\gamma < 2.5, \quad (23)$$

and, for $\tilde{c}_\gamma < 0$:

$$-0.1 < \tilde{c}_g/\tilde{c}_\gamma < -0.065, \quad -0.016 < \tilde{c}_g/\tilde{c}_\gamma < 0.001. \quad (24)$$

¹⁰ Note that these bounds are approximate in the following sense: for a 1D fixed relationship between the Wilson coefficients, the allowed C.L. regions are slightly different if obtained with the 1D CDF or for the 2D Wilson coefficient case. Again, this effect can be seen in the NSUSY case in Fig. 1

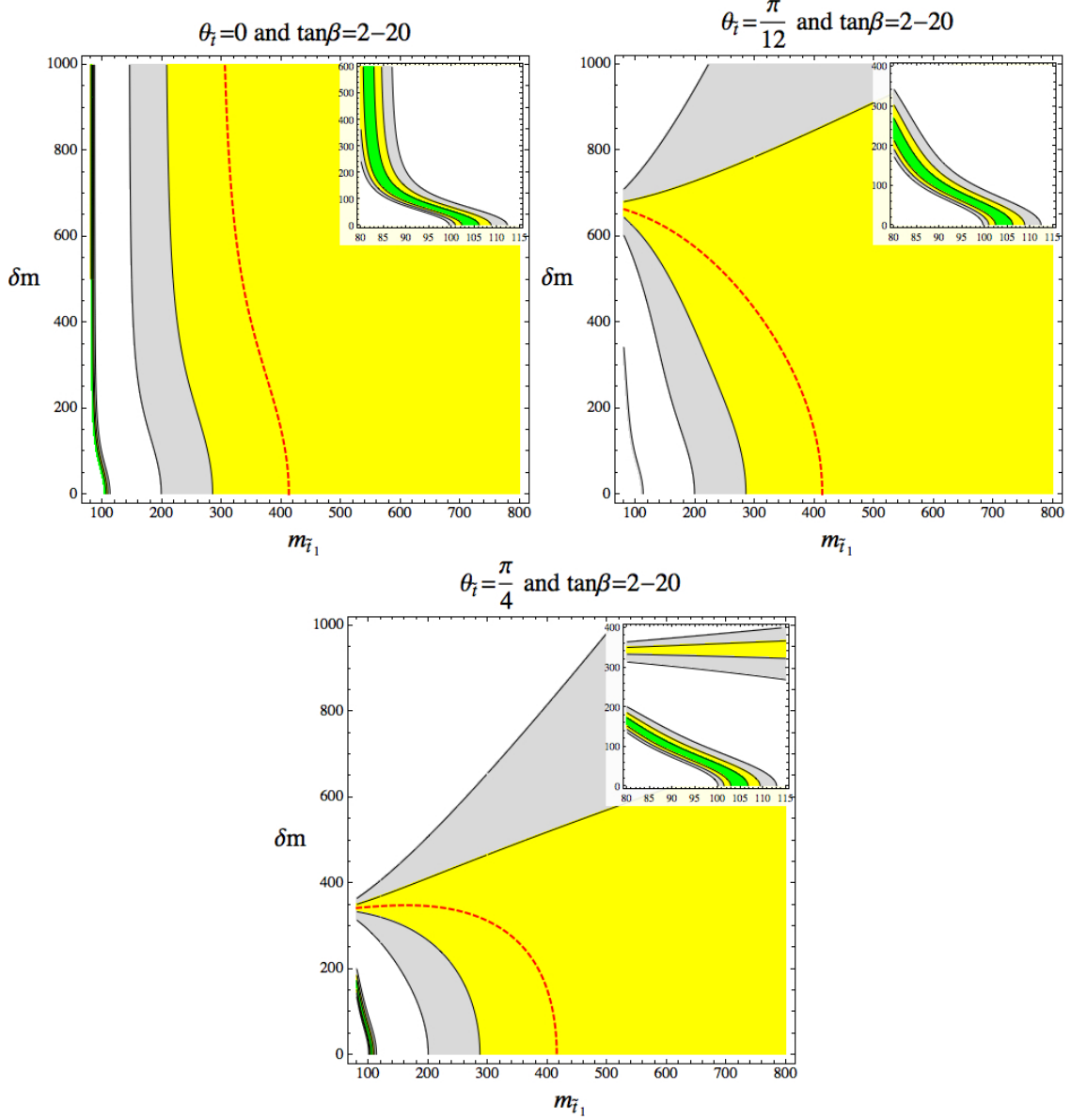


FIG. 2: The projection into stop parameter space of the best-fit regions from a global fit to Higgs signal strength data. Here $\delta m = (m_{\tilde{t}_2}^2 - m_{\tilde{t}_1}^2)^{1/2}$. Colour convention is the same as in previous plots. The inset zooms into the low mass best-fit region (ruled out by LHC monophoton searches). We have varied $\tan\beta$ in the range $(2, 20)$ and taken the overlap of the best fit spaces, slightly increasing the allowed parameter space. The three plots show the cases of no mixing ($\theta_{\tilde{t}} = 0$), intermediate mixing ($\theta_{\tilde{t}} = \pi/12$) and maximal mixing ($\theta_{\tilde{t}} = \pi/4$). The dashed line corresponds to the second minimum in the one parameter χ^2 shown in the previous figure.

In the limit of a single field contributing to the Wilson coefficients, the $\tilde{c}_g/\tilde{c}_\gamma$ ratio is dictated by the quantum numbers of the field integrated out.¹¹ Clearly, the study of the possible intersections of such lines with the best-fit regions in the space $(\tilde{c}_g, \tilde{c}_\gamma)$ for any model (including NSUSY) will become much more important with further refinements in the measurement of Higgs properties. We discuss some prospects for the improvement of these fits in Section VI.

For the NSUSY case, the light stop best-fit region occurs for $F_g \sim 2$; one can see how this space relates to the $(\tilde{c}_g, \tilde{c}_\gamma)$ plane in Fig. 1, and it corresponds to stops significantly lighter than in the region of small F_g . This space is already strongly constrained by monophoton searches, as we discuss further below. NSUSY hopes in light of current global Higgs data (when our assumptions are adopted) are based on the consistency of NSUSY in the $(\tilde{c}_g, \tilde{c}_\gamma)$ parameter space near the SM point $(\tilde{c}_g, \tilde{c}_\gamma) = (0, 0)$, for larger $m_{\tilde{t}_1}$ and small F_g . Translating the allowed fit space to the space of the stop parameters is very convenient to discuss the interplay with further constraints and direct stop discovery prospects. When we translate the results of the global fit to Higgs signal-strengths to the stop space, we find the best-fit regions shown in Fig. 2. The three plots show the cases of no mixing ($\theta_{\tilde{t}} = 0$), intermediate mixing ($\theta_{\tilde{t}} = \pi/12$) and maximal mixing ($\theta_{\tilde{t}} = \pi/4$). We will show these canonical parameter choices throughout this paper when examining the global constraint picture. The point in the 1D fit that has a local minimum χ^2 with small F_g is mapped into the red dashed line in each of the stop space plots in Fig. 2 and, as expected, has larger $m_{\tilde{t}_1}$. As anticipated, the best-fit region at low stop-mass is extremely narrow: a sure indication of its fine-tuned nature.

C. $\text{Br}(\bar{B} \rightarrow X_s \gamma)$

Another important challenge for the parameter space of NSUSY scenarios comes from non-SM contributions to magnetic moment operators. Although the contributions to these operators vanish [43] in the pure SUSY limit, NSUSY scenarios are far from this limit by construction. As a result, the reduction in the allowed parameter space due to constraints from $\text{Br}(\bar{B} \rightarrow X_s \gamma)$ can be

¹¹ See Ref. [42] for a recent study that also emphasizes this point.

significant. Recall that the effective Lagrangian (neglecting light quark masses) is given by [44]

$$\begin{aligned}\mathcal{L}_{eff} &= \frac{4G_F}{\sqrt{2}} V_{tb} V_{ts}^* \sum_{i=1}^8 C_i(\mu) Q_i, \\ &= \frac{G_F}{4\sqrt{2}\pi^2} V_{tb} V_{ts}^* m_b \left[C_7 \bar{s}_L \sigma^{\mu\nu} b_R e F_{\mu\nu} + C_8 \bar{s}_L \sigma^{\mu\nu} T_a b_R g_s G_{\mu\nu}^a + \dots \right].\end{aligned}\quad (25)$$

The SUSY contributions to the magnetic moment operators are well known [45] and can be applied to the particular NSUSY scenario. The dominant contributions to the Wilson coefficients come from stop-chargino loops:

$$\Delta C_{7,8} \simeq \sum_{i=1}^2 \left\{ -|\langle \tilde{t}_i | \tilde{t}_R \rangle|^2 \frac{m_t^2}{3 s_\beta^2 m_{\tilde{t}_i}^2} F_{7,8}^1 \left[\frac{m_{\tilde{t}_i}^2}{m_{\chi_1}^2} \right] - \langle \tilde{t}_i | \tilde{t}_L \rangle \langle \tilde{t}_R | \tilde{t}_i \rangle \frac{m_t}{2 s_{2\beta} m_{\chi_1}} F_{7,8}^3 \left[\frac{m_{\tilde{t}_i}^2}{m_{\chi_1}^2} \right] \right\}. \quad (26)$$

We have only retained the light χ_1^\pm with mass $m_{\chi_1^\pm} \simeq \mu$ as consistent with NSUSY assumptions (the gaugino mass is $M_2 > \mu \gtrsim m_W$). The loop functions $F_{7,8}^j$ are given in the Appendix. We vary the μ parameter in the range $\sim 100 - 200$ GeV. The lower limit of this range is set by LEP bounds on $\tilde{\chi}^\pm$ [46]; the upper limit by naturalness considerations [6]. In principle, there are also loop contributions from the light χ^0 . However, these contributions can be strongly suppressed in the minimal NSUSY limit we consider. For example, there is no source of breaking of the residual $U(1)_R$ symmetry, unless Majorana masses for the gluino are introduced. This symmetry plays a role in suppressing effects of large $\tan \beta$ or proton decay or flavour violating observables which require a flip in chirality, see Refs [47, 48]. We will consider a minimal flavour violating scenario [49–53] when examining the NSUSY spectrum, this can follow from the argument above directly. In the case of Majorana gluino masses we assume MFV.

We use the results of Ref. [54] for the constraints on the BSM Wilson coefficients $C_i = C_i^{SM} + \Delta C_i$ set by the observable $\text{BR}(\bar{B} \rightarrow X_s \gamma)_{E_\gamma > 1.6 \text{ GeV}}$. The contribution of the BSM Wilson coefficients to this observable is given by

$$\text{BR}(\bar{B} \rightarrow X_s \gamma)_{E_\gamma > 1.6 \text{ GeV}} = [(3.15 \pm 0.23) - 8.0 \Delta C_7(\mu_0) - 1.9 \Delta C_8(\mu_0)] \times 10^{-4}. \quad (27)$$

Here we neglect $(\Delta C_i)^2$ terms and have used (implicitly) the input values listed in Ref. [54], where, in particular, the scale $\mu_0 = 160$ GeV was chosen for the SM results. Another assumption used in Ref. [54] is that all other induced BSM operators have Wilson coefficients that satisfy

$$\frac{C(\mu \sim \mu_0)}{G_F \Lambda} \sim \mathcal{O}(g_W^n), \quad n \geq 2, \quad (28)$$

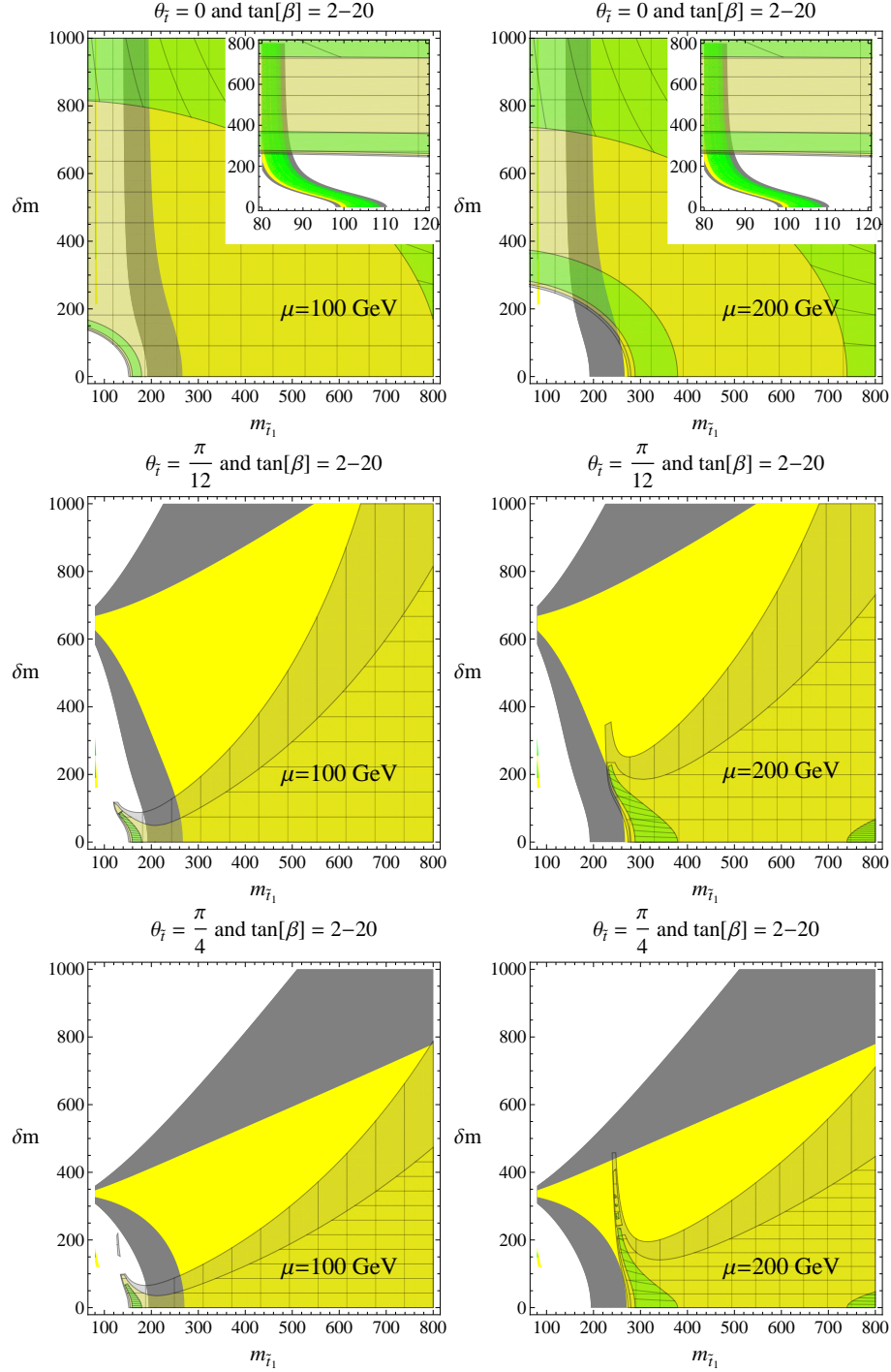


FIG. 3: Overlay of the best-fit regions of stop parameter space from global fit to Higgs signal strength data with the allowed space due to $\text{Br}(\bar{B} \rightarrow X_s \gamma)$ at the level of 1, 2, 3 σ . The 3 σ allowed region is overlaid with a vertical mesh, the 2 σ has a horizontal and vertical mesh, while the 1 σ allowed region is the green region with the further addition of the diagonal mesh.

and the NSUSY scenarios we are interested in will have to satisfy this condition when this constraint is strictly applied. Comparing to the current world experimental average given in Ref. [55]

$$\text{BR}(\bar{B} \rightarrow X_s \gamma)_{E_\gamma > 1.6 \text{ GeV}} = [3.55 \pm 0.24 \pm 0.09] \times 10^{-4}, \quad (29)$$

we will use the $1(2)\sigma$ bound $-8.0 \Delta C_7 - 1.9 \Delta C_8 = 0.3 \pm 0.34(0.69)$ to constrain the NSUSY parameter space.¹² In Fig. 3 we show the interplay of the constraints from the global fit to Higgs data and constraints due to $\text{Br}(\bar{B} \rightarrow X_s \gamma)$ in minimal NSUSY. We see that there exists consistent parameter space that can pass both experimental tests, primarily at the level of $\sim 2\sigma$ in each case. Large mass splittings scenarios of the stop states when large mixing is present are significantly disfavoured.

D. Electroweak Precision Data

Measurements of m_W and other EW precision observables also restrict the allowed parameter space of the NSUSY scenario. Recent measurements of m_W at the Tevatron [57, 58] are of particular interest. The world average [59] has been refined to $(m_W)_{\text{exp}} = 80.385 \pm 0.015 \text{ GeV}$, with a significant reduction of the quoted error. As recently re-emphasized in Refs. [60, 61], precise measurements of the value of m_W constrain the allowed parameter space of a weak scale NSUSY spectra when m_h is known. This occurs as the allowed custodial symmetry violation that could be present in the sfermion sector is bounded. Note that a global fit to EWPD produces a ΔT constraint that has about twice the error of the constraint used here, which is directly determined from the shift in the W mass.

In this Section, we add this further constraint in the study of the impact of NSUSY spectra on Higgs properties. We use the numerical approximation of the two-loop SM prediction of m_W given by Ref. [62] and the method of Ref. [61]. The relevant SUSY correction to the SM prediction¹³ of m_W is given in Refs. [63–66] as

$$(\Delta m_W)^{\text{SUSY}} \simeq \frac{m_W c_W^2}{2(c_W^2 - s_W^2)} \Delta \rho^{\text{SUSY}}. \quad (30)$$

¹² We are aware of the recent Babar result, $\text{BR}(\bar{B} \rightarrow X_s \gamma)_{E_\gamma > 1.6 \text{ GeV}} = [3.31 \pm 0.16 \pm 0.30 \pm 0.10] \times 10^{-4}$, Ref. [56], with a lower central value but larger error. As this result is not yet incorporated into a global average, we use the quoted HFAG average.

¹³ Here s_W is defined in the on-shell scheme.

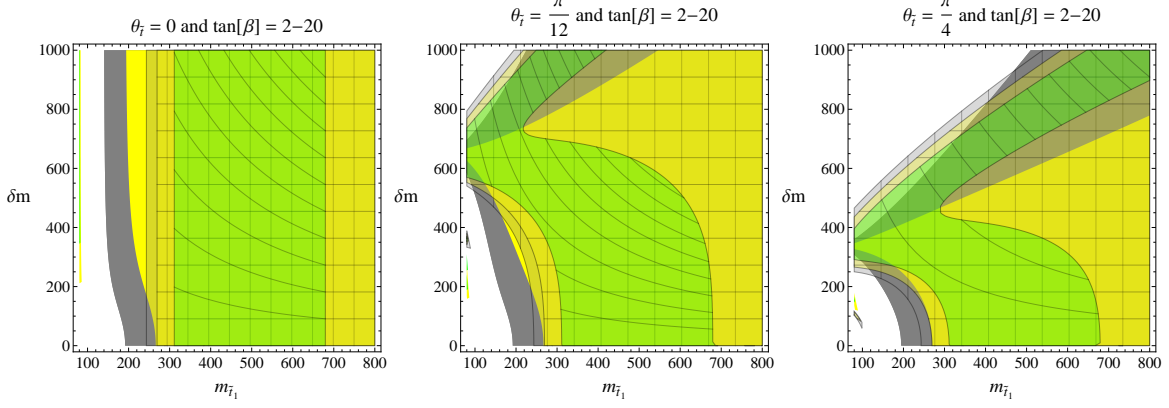


FIG. 4: Constraints from precision measurements of m_W , shown as 1, 2, 3 sigma shaded regions, overlaid on the allowed stop parameter space consistent with the global fit to Higgs signal strength data. Plot colour/display convention is the same as in previous figures.

Neglecting terms proportional to small \tilde{b} mixing angles, the SUSY contribution is given by

$$\Delta\rho_0^{SUSY} \simeq \frac{3 G_F}{8 \sqrt{2} \pi^2} \left\{ \sum_{i=1,2} |\langle \tilde{t}_L | \tilde{t}_i \rangle|^2 F_0[m_{\tilde{t}_i}^2, m_{\tilde{b}_L}^2] - |\langle \tilde{t}_L | \tilde{t}_1 \rangle|^2 |\langle \tilde{t}_L | \tilde{t}_2 \rangle|^2 F_0[m_{\tilde{t}_1}^2, m_{\tilde{t}_2}^2] \right\}, \quad (31)$$

and the function F_0 is defined as

$$F_0[x, y] = x + y - \frac{2xy}{x-y} \log \frac{x}{y}. \quad (32)$$

We can trade $m_{\tilde{b}}$ in this expression for the stop masses and the stop mixing angle ($\theta_{\tilde{t}}$) using

$$m_{\tilde{b}_1}^2 \simeq \cos^2 \theta_{\tilde{t}} m_{\tilde{t}_1}^2 + \sin^2 \theta_{\tilde{t}} m_{\tilde{t}_2}^2 - m_t^2 - m_W^2 \cos(2\beta). \quad (33)$$

This assumes small sbottom mixing and neglects perturbative corrections. We are also neglecting other SUSY contributions to $\Delta\rho^{SUSY}$, namely the $\chi^{\pm,0}$ contributions from the light states retained in the residual NSUSY spectrum. The masses of these states are set by the same scale ($\sim \mu$) in NSUSY, and the mass splitting of these doublets is small, leading to subdominant contributions to $\Delta\rho^{SUSY}$. In order to define the SM prediction of m_W we must specify a central value and error in m_h . Given the current state of the data we simply take the Higgs mass range 125 ± 2 GeV for this constraint. The effect of this uncertainty in m_h is very subdominant to the largest source of error, which is the uncertainty in m_t (which leads to a ± 5.4 MeV effect on m_W).

With the choice of input parameters in Table II, we find $(m_W)_{SM} = 80.368 \pm 0.006$ GeV, which constrains NSUSY through the resulting bound $(\Delta m_W)^{SUSY} \lesssim 0.023 \pm 0.016$ GeV. This

translates into a constraint $\Delta\rho^{SUSY} \lesssim (4.1 \pm 2.8) \times 10^{-4}$. This is in good agreement with the result of Ref. [61], which uses the same method, up to small differences in the input parameters.

Note that for $\theta_{\tilde{t}} > \pi/4$ the lightest stop is dominantly \tilde{t}_R compared to the interval we discuss, $0 < \theta_{\tilde{t}} < \pi/4$, in which it is dominantly \tilde{t}_L . However, in the former case one still obtains a similar constraint space for the Δm_W constraint, with the shift in the SM prediction and the best fit value selecting for degenerate stop states.

1. The Funnel Region

We show the overlap of the global Higgs fit constraints and the constraints due to m_W in Fig. 4. Note the good degree of consistency between both constraints. This consistency can be traced to the following. The low mass “funnel region” in stop parameter space arises from minimizing the contribution to F_g . The condition $F_g \rightarrow 0$ translates into the relationship

$$\sin(2\theta_{\tilde{t}}) \simeq \frac{2m_t(m_{\tilde{t}_1}^2 + m_{\tilde{t}_2}^2)^{1/2}}{(m_{\tilde{t}_2}^2 - m_{\tilde{t}_1}^2)^2}. \quad (34)$$

Using this constraint in the maximal mixing case, and substituting into the $\Delta\rho_0^{SUSY}$ expression, one finds (expanding in $m_t/m_{\tilde{t}_2} < 1$)

$$\Delta\rho_0^{SUSY} \simeq \frac{3G_F}{8\sqrt{2}\pi^2} \left(\frac{m_t^4}{3m_{\tilde{t}_2}^2} \right) \left[1 + \frac{m_t^2}{2m_{\tilde{t}_2}^2} \dots \right]. \quad (35)$$

This corresponds to a suppression of $\Delta\rho_0^{SUSY}$ to the right order of magnitude to match the condition $\Delta\rho^{SUSY} \sim 10^{-4}$. This basic correlation also occurs outside of the maximal mixing case we have considered for simplicity, although the above equation is modified by $O(1)$ numerical coefficients. Conversely, when the stop parameters are not related in this manner, $\Delta\rho_0^{SUSY}$ receives a contribution dominated by the largest mass scale

$$\Delta\rho_0^{SUSY} \simeq \frac{3G_F}{8\sqrt{2}\pi^2} (m_{\tilde{t}_1}^2, m_{\tilde{t}_2}^2) \quad (36)$$

and is significantly larger, ruling out the associated parameter space. In this sense, this region is clearly associated with some cancelations due to parameter tuning.

E. Collider Bounds

In this Section we describe some of the current collider bounds on the NSUSY spectrum and how they pertain to the stop parameter space of interest found in previous sections. The most stud-

ied and stringent bounds on NSUSY come from missing energy signatures. However, including R-parity or not in a weak scale NSUSY spectrum is not dictated directly by naturalness. Due to this, we will mostly restrict our attention to more robust collider constraints. We note however that with the absence (to date) of missing energy signatures, several searches for R-parity violating phenomenology (without significant missing energy) [18] in the multijet and multilepton final states are now ongoing. These studies could further constraint the interesting parameter space that we isolate in this study.

The main features of NSUSY relate to the Higgsino and Stop sectors. As we have discussed before, if Higgsinos get their mass solely from the μ term, we expect a very small mass splitting between the χ^\pm, χ^0 , of the order of $\mathcal{O}(v\mu/M_{1,2}^2)$. Here $M_{1,2}$ are the gaugino masses that are taken to be large $M_{1,2} \gg v$ in minimal NSUSY. In the deep-Higgsino region, the $\chi^\pm \rightarrow \chi^0 + X$ decay occurs with no hard- p_T objects to tag on. Then, only monojet/monophoton searches at LEP were sensitive to such decays, leading to a bound $m_{\tilde{\chi}^\pm} > 92$ GeV [46].

Searches for stops are limited by the complexity of the final state and the similarity with the SM $t\bar{t}$ background, especially in a scenario where the chargino and neutralino are heavy. The recent direct stop combination searches from ATLAS [67] do not have sensitivity on the stop mass, except in a very small region around $m_{\tilde{t}} \sim 300$ GeV, and only for a limited range of μ .¹⁴ One can obtain more information on the stop sector by looking at searches of a single photon plus missing energy [72, 73]. Although those searches were performed in the context of large extra-dimensions and dark matter effective theories, a straightforward re-interpretation in terms of SUSY can be done [74], within the assumption that the stop and the neutralino are separated by ≤ 30 GeV. This is indeed the case in the low-mass region preferred by the Higgs fit, namely $m_{\tilde{t}} \leq 120$ GeV. Since the Higgsino is heavier than 90 GeV, the splitting between $\tilde{\chi}$ and \tilde{t} is right at the best sensitivity point. The mass bound obtained in Ref. [74] is 150 GeV (95% C.L.). This strongly constrains/excludes the low mass stop parameter space most preferred in the global Higgs fits. Monojet searches could also be used in the low $m_{\tilde{t}_1}$ region of parameter space [75], and one could also use top precision measurements (spin correlations) to rule out this area of parameter space [69].

Finally, we note that gluino-assisted stop production searches rely on a light gluino around a

¹⁴ Note that there are some proposals to improve the stop searches [68–71], using different strategies, from boosted tops to fitting the missing energy distribution.

TeV, which is in some tension with the combination of multijets+leptons+missing energy [76, 77], which leads to a bound of 1050 GeV. This gluino bound is rather model independent, as intermediate $\tilde{\chi}^\pm$, $\tilde{\chi}_2$ to leptons or off-shell stops do not change the bound considerably [78, 79].¹⁵ Nevertheless, a gluino heavy enough to disable this search is allowed in a minimal NSUSY scenario and the stop limits from these gluino-assisted studies do not (as yet) directly constrain the parameter space of interest.

V. COMBINING CONSTRAINTS

It is of interest to address how an NSUSY scenario globally fits the increasingly rich dataset. In past sections, we have shown the interplay of various precision constraints; in this Section we perform a global χ^2 fit to Higgs signal-strength data, constraints due to precision measurements of m_W and $\text{Br}(\bar{B} \rightarrow X_s \gamma)$. We fix $\tan \beta = 10$ and show in Fig. 5 such global fit results for the three mixing cases we have considered in this paper, to illustrate the allowed global fit space.

The results in Fig. 5 show a good fit to the data. We are fitting to fifty observations: forty-eight Higgs signal-strength measurements, as well as Δm_W and $\text{Br}(\bar{B} \rightarrow X_s \gamma)$. For the three mixing cases $\theta_{\tilde{t}} = 0, \pi/12, \pi/4$ and $\mu = 100, 200$ GeV we find, fitting to the two stop parameters $m_{\tilde{t}_1}, \delta m$, that $\chi^2_{\min}/(50 - 3) \simeq 1$. The interplay of the constraints that allows a good fit is of interest. The best-fit region in the Higgs signal-strength fit at very low masses, $m_{\tilde{t}_1} \sim 100$ GeV, is essentially ruled out due to mono-photon searches and constraints from Δm_W and $\text{Br}(\bar{B} \rightarrow X_s \gamma)$. When combining constraints, one finds a best fit to the Higgs signal-strength data with a larger $m_{\tilde{t}_1}$ (with less mass splitting for larger $\theta_{\tilde{t}}$) in a manner that also improves agreement with the small deviations from the SM predictions in Δm_W for large regions of parameter space. However, the significance of this observation is currently marginal: the SM gives a comparable fit to these observables with $\chi^2_{\min}/(47) \simeq 1.0$.

A. Fine-tuning and the Higgs Mass

It is also interesting to examine if the Higgs mass could be consistent with its observed value in the allowed parameter space of the fit, without large fine-tuning. We have included the large

¹⁵ Although this search is optimized for Majorana gluinos, the limit would be even more stringent for Dirac gluinos [80].

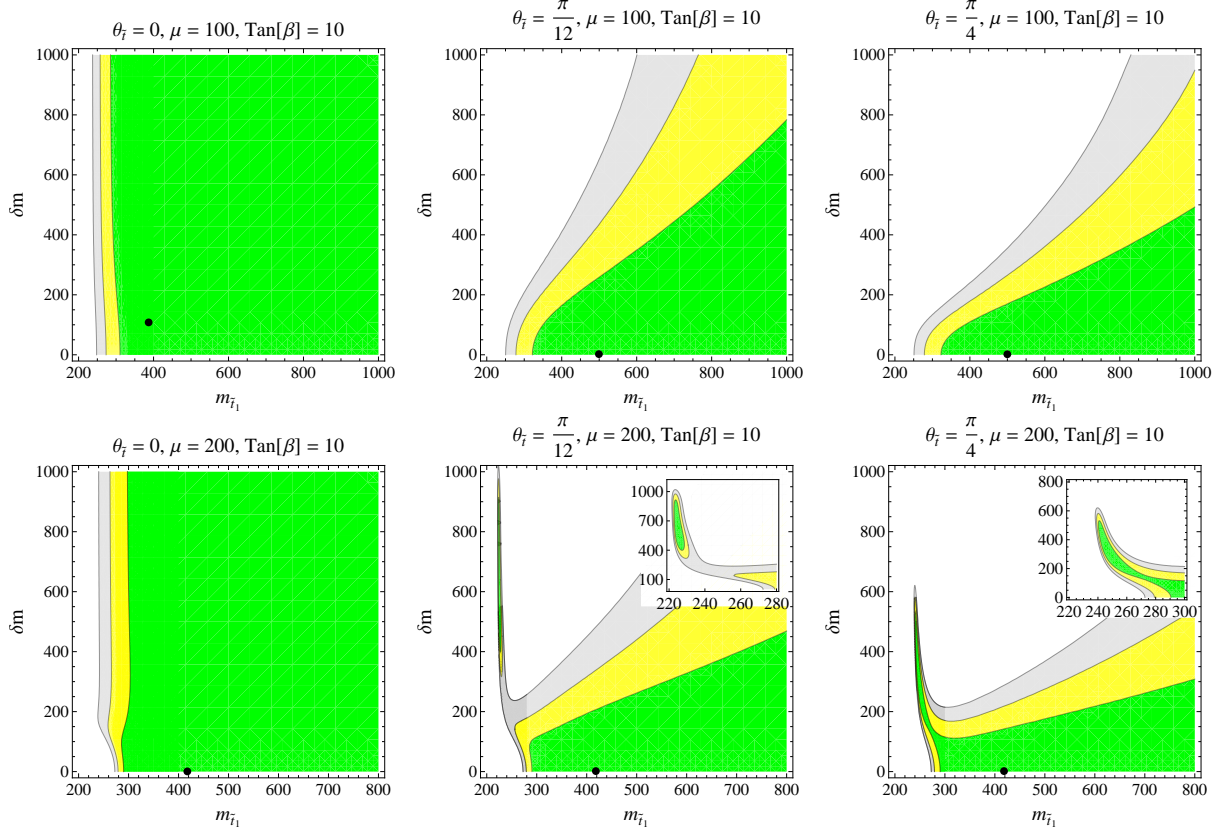


FIG. 5: Best-fit regions in stop parameter space from the global χ^2 . Colour conventions the same as in previous figures. We show the three mixing cases $\theta_{\tilde{t}} = 0, \pi/12, \pi/4$ for two values of μ that set the Higgsino mass scale in these minimal scenarios, $\mu = 100, 200$ GeV. The $\tan\beta$ dependence of the result is primarily driven by the $\text{Br}(\bar{B} \rightarrow X_s \gamma)$ constraint. Larger values of $\tan\beta$ select for a more degenerate stop spectrum when $\theta_{\tilde{t}} \neq 0$. In determining χ^2_{\min} , we have assumed a prior $150 \text{ GeV} \leq m_{\tilde{t}_1}$, due to monophoton constraints. In each figure the best fit point is marked with a dot.

radiative corrections to the Higgs mass expected after SUSY breaking [81] by using the public code FeynHiggs [82, 83] (for alternatives, see [84]), which includes all one-loop corrections and the dominant two-loop effects [85]. This gives a precise enough determination of m_h (with an error of a few GeV), provided the hierarchy in the stop masses is not so large that further re-summation of logarithms is needed [86]. Precision is needed here because the soft masses required to give a large enough Higgs mass are exponentially sensitive to m_h .

We show in Fig. 6 the band in stop parameter space that gives $m_h = 125 \pm 2 \text{ GeV}$, overlaid on the best fit regions. The Higgs mass has a non-negligible two-loop sensitivity to the value of

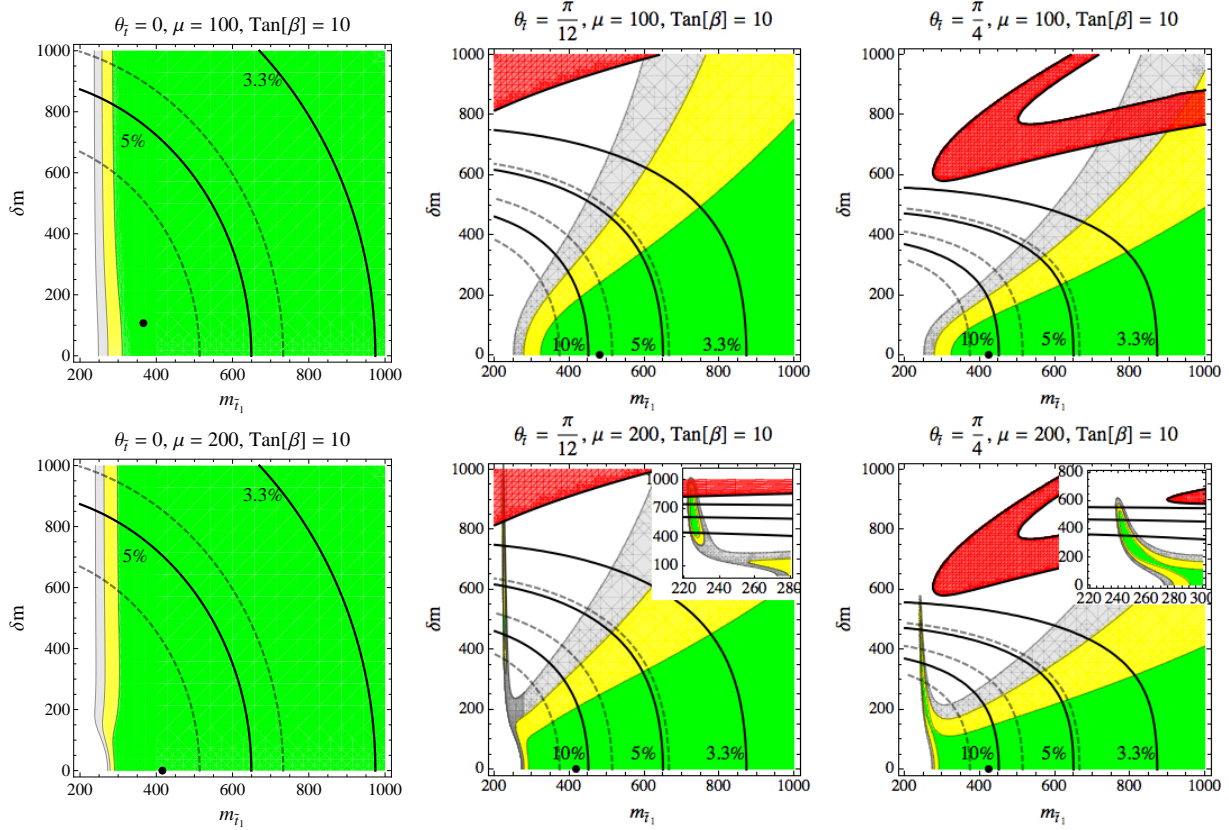


FIG. 6: The overlay of the Higgs mass condition $m_h = 125 \pm 2$ GeV (in red/darker shaded region) and the best fit space (colour convention the same as in previous figures). Also shown are labeled contours of constant fine-tuning (solid black) for a UV cutoff $\Lambda = 10$ TeV. The same contours are shown (dashed grey) for $\Lambda = 50$ TeV. In the no-mixing case, the Higgs mass constraint cannot be accommodated in minimal scenarios: no Higgs mass band is present in these plots.

the gluino mass, which we have chosen to be 1.1 TeV in this figure.¹⁶ For non-zero stop mixing, larger values of the gluino mass tend to lower m_h and therefore require larger values of the stop masses [82]. We see in Fig. 6, left plot, that the best-fit region with sub-TeV stop masses and zero mixing is not consistent with the Higgs mass condition, as was to be expected. Larger stop masses with large mixing can however produce the observed Higgs mass value (Fig. 6, middle and right plot) in exceptional regions of parameter space (or when a worse fit is considered), although the degree of fine-tuning in these parameter regions is a concern.

It is well known that physics beyond the minimal supersymmetric version of the SM can easily

¹⁶ We take the other sfermion states to be ~ 2 TeV in this analysis, however the Higgs mass band is insensitive to the particular mass values of these states for $\tan \beta \sim 10$ and sfermion masses in the TeV range.

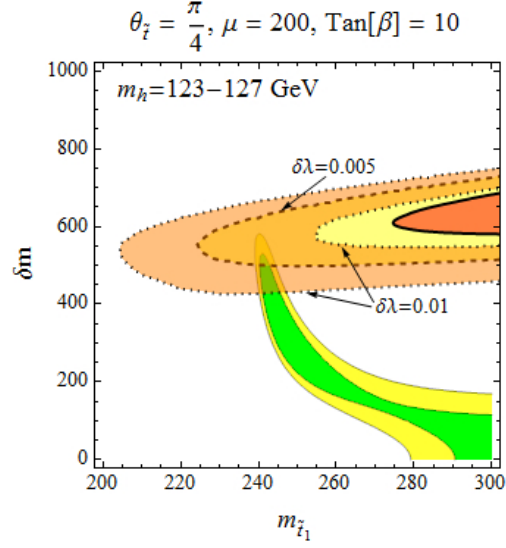


FIG. 7: Effect of an upward shift on the Higgs quartic, $\delta\lambda$ on the allowed Higgs mass band $m_h = 125 \pm 2$ GeV. We have chosen the stop parameters as for one of the cases of the previous figure, see inset of lower right plot. The corresponding Higgs mass band is the small red region on the right. For $\delta\lambda = 0.005$ (0.01) this region extends to lower stop mass values and is given by the faded yellow (orange) band bounded by a dashed (dotted) line, as indicated.

give contributions to the Higgs quartic coupling which controls the Higgs mass. This can happen through new sectors coupled to the Higgs in such a way that they add at tree-level new supersymmetric F -term or D term (or even susy-breaking) contributions to the Higgs quartic even in the Higgs decoupling limit (see [87–89] for an incomplete list of studies on this). A very moderate tree-level upward shift of this quartic, which can be interpreted as a threshold correction at the SUSY scale, would have a direct and very important impact on increasing the predicted Higgs mass and reducing the associated fine-tuning. We have illustrated this in Fig. 7, which assumes an additional contribution $\delta\lambda = 0.005, 0.01$ to the Higgs quartic coupling $\lambda = m_h^2/(2v^2)$. The new physics required for this shift can, on the other hand, have a negligible impact on the coupling of the Higgs to gluons or photons. Therefore, in such scenarios one is allowed to soften the link between m_h and the stop sector, while the analysis of the impact of Higgs search results on constraining stop parameters we have performed would still apply.

It is difficult to define a uniquely compelling fine-tuning measure in an effective theory, or argue what degree of fine-tuning is clearly unacceptable. Fine-tuning considerations are necessarily dependent on the UV physics of the EFT and so one can only make a rough estimate in a low-

energy effective theory. We could follow the definition of fine-tuning measure of [90, 91], which quantifies the tuning by measuring the sensitivity of the electroweak scale (as given by e.g. the Z mass) with respect to changes in the fundamental UV parameters. However, as we want to keep an open mind about what detailed UV physics completes the NSUSY scenario, we will content ourselves with a different estimate of tuning that simply compares the value of the Z mass with known loop contributions to it (in our case those coming from stop corrections), requiring that the latter are not much bigger than m_Z . That is, defining

$$\Delta_Z = \left| \frac{\delta_{\tilde{t}} m_Z^2}{m_Z^2} \right|, \quad (37)$$

the associated fine-tuning will be 1 part in Δ_Z . Restricting ourselves to the moderate value of $\tan \beta \sim 10$ and assuming that stops loops are the dominant contribution to this fine-tuning measure, one finds (see e.g. [92])

$$\begin{aligned} \delta_{\tilde{t}} m_Z^2 &\simeq \frac{3m_{\tilde{t}}^2}{4\pi^2 v^2} \left(M_{\tilde{Q}_L}^2 + M_{\tilde{t}_R}^2 + A_t^2 \right) \log \left(\frac{2\Lambda^2}{m_{\tilde{t}_1}^2 + m_{\tilde{t}_2}^2} \right) \\ &\simeq \frac{3}{8\pi^2 v^2} \left[2m_{\tilde{t}}^2(m_{\tilde{t}_1}^2 + m_{\tilde{t}_2}^2 - 2m_t^2) + \frac{1}{4}(\delta m)^4 \sin^2(2\theta_{\tilde{t}}) \right] \log \left(\frac{2\Lambda^2}{m_{\tilde{t}_1}^2 + m_{\tilde{t}_2}^2} \right). \end{aligned} \quad (38)$$

The scale Λ is associated with new states required to cut off the logarithmic divergence in the effective theory, and is associated with the messenger scale that transmits SUSY breaking from a hidden sector. The choice of this scale is UV dependent, offering some further caution on the interpretation of the results. For numerical purposes we consider this scale to be $\Lambda \sim 10, 20$ TeV consistent with recent choices in the literature [6]. The fine-tuning contours are overlaid in Fig. 6 in this case (for related work, see Ref. [93]).

It is interesting to note the exceptional region of parameter space in the global χ^2 that allows the Higgs mass to be raised with relatively light stops and smaller fine-tuning, see Figs. 6 and 7 for $\mu = 200$ GeV (light stop mass insets). This is another example of the “Funnel region” of stop parameter space. The $\text{Br}(\bar{B} \rightarrow X_s \gamma)$ constraint is sensitive to this region of parameter space, and we note that although currently allowed with the HFAG average we have used, incorporating the recent Babar update into the a global average of $\text{Br}(\bar{B} \rightarrow X_s \gamma)$ will further resolve this interesting region of parameter space. We also note that, if this parameter space continues to offer a good fit to the data, such stop masses are very difficult to probe directly in collider searches. A continued deviation consistent with such stop parameters in the global Higgs fits could be the leading experimental indication of the presence of stop states in this exceptional region of parameter space. We discuss the prospects for such future fits in the next Section.

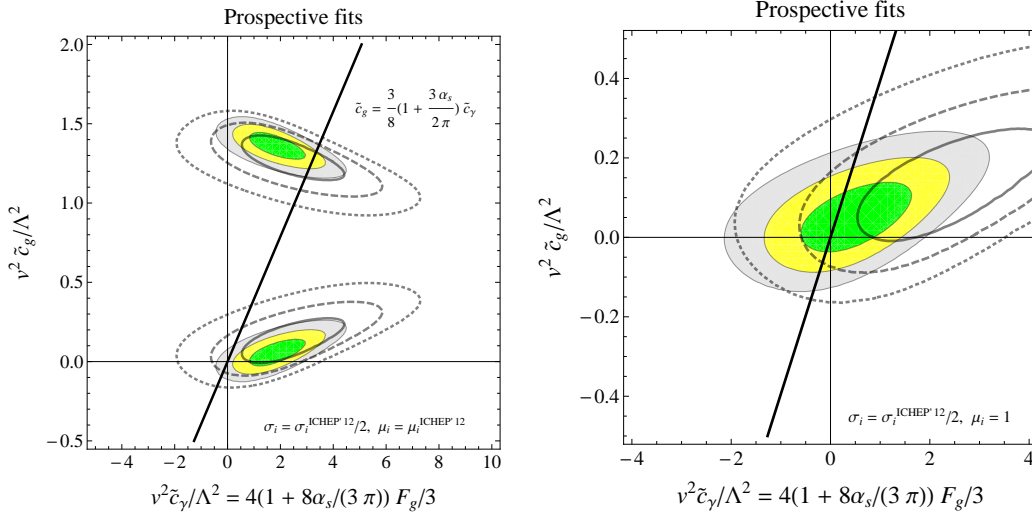


FIG. 8: Projected best-fit areas when 8 TeV signal-strength values hypothetically report by the end of 2012 have their errors scale down to $\sigma_i/2$ while they keep their current 8 TeV best-fit central values (left) and when the best-fit central values converge to the SM (right). For comparison, we also show in faded gray (solid, dashed, dotted) lines the current $(1, 2, 3) \sigma$ best-fit contours.

VI. PROJECTIONS FOR NSUSY AT THE END OF THE 8 TEV RUN

A. Fit prospects.

The integrated luminosity of experiments at LHC is increasing at a rapid pace, and the power and precision of global Higgs fits of this form have scaled remarkably to date in the 7, 8 TeV runs. If this scaling continues (i.e. if systematics and/or correlations do not become the dominant source of error by the end of this year) and each experiment gathers the projected $\sim 30 \text{ fb}^{-1}$ before shutdown, we can study the NSUSY prospects for fits of this form by the end of the 8 TeV run. We reduce each of the reported 8 TeV signal strength errors by a factor 2, down to $\sigma_i/2$, and assume two different scenarios for the final 8 TeV $\hat{\mu}_i$ central values: 1) they retain their current central values, or alternatively, 2) they move to $\hat{\mu}_i = 1$. As the integrated luminosity is to increase by more than a factor of four while more channels are also expected to be added to the global Higgs dataset, this estimate is conservative. We show the prospective best-fit regions in the two dimensional Wilson coefficient space of the hgg and $h\gamma\gamma$ operators in these two hypothetical cases in Fig. 8. It is clear that a much more constrained stop space due to these Higgs fits, and possibly a $1 - 2\sigma$ exclusion of NSUSY, will be feasible by the end of the 8 TeV run. Due to decoupling,

if the SM emerges as a better fit in the dataset, with $\hat{\mu}_i^{8\text{TeV}} \rightarrow 1$, NSUSY will be relatively less constrained by fits of this form, however, fine-tuning arguments could be used against it.

B. Prospects for bounding the best-fit regions: collider and Higgs search exclusions

In this Section we compare the impact of the global fit on the stop parameter space with the searches based on missing energy. The global fit we have performed with NSUSY draws interesting conclusions: light and nearly degenerate stops are preferred in the range of 400-500 GeV and there is an exceptional region of parameter space with even lighter stops. These regions accommodate the global Higgs properties and the m_W and $\text{Br}(\bar{B} \rightarrow X_s \gamma)$ constraints. On the other hand, if the value of the Higgs mass is due solely to the stop sector, the allowed region shifts. Somewhat heavier stops, with a larger separation ($\gtrsim 200$ GeV) seem to be indicated in this case, mostly outside of the exceptional region of parameter space. The same fit to Higgs data does rule out a small portion of the stop parameter space, comparable to the monophoton exclusion. Note however, that those two exclusions, from monophoton searches and from Higgs data, have different degrees of SUSY model dependence. The monophoton exclusion is based on missing energy signatures due to assumed R-parity conservation, whereas the Higgs data exclusion does not assume it, or any particular stop decay chain.

In the experimental searches, stops are assumed to decay to $\chi^{\pm,0}$. In the case of NSUSY, those electroweak states are degenerate higgsinos, leading in both cases to missing energy in association with a b-jet or a top,

$$\begin{aligned}\tilde{t} &\rightarrow b \tilde{\chi}^+ \rightarrow b \tilde{\chi}^0 + \text{soft objects} \\ \tilde{t} &\rightarrow t \tilde{\chi}^0.\end{aligned}\tag{39}$$

The first decay chain corresponds to the direct sbottom search [60, 94–97]. The second decay chain contains a top (on or off-shell), considered by the direct stop searches by ATLAS (See Sec. IV E).

The current stop searches are very weak in the region of $m_{\tilde{\chi}^0} \sim \mu > 90$ GeV. The current ATLAS exclusion region is a small triangle below $\mu = 160$ GeV, and between, roughly, 300 and 450 GeV. To explore NSUSY in this best-fit region, one would need to push the stop searches not towards larger values of $m_{\tilde{t}}$, but of $m_{\tilde{\chi}^0}$. The main issue to reach higher values of μ is the similarity with $t\bar{t}$ when either for $m_{\tilde{t}} \sim m_t + \mu$, or large μ . In both cases, the missing energy distribution loses its ability to suppress the top background. The stop has little phase space to

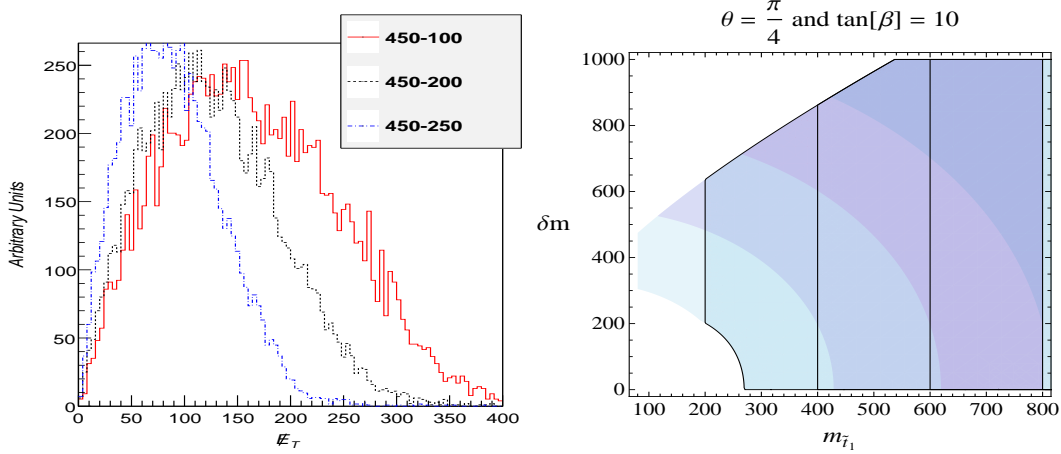


FIG. 9: Left figure: The missing energy distribution for different choices of neutralino mass, with the stop mass fixed to 450 GeV. The red-solid, black-dotted and blue-dashed lines correspond to $m_{\tilde{\chi}}=100, 200$ and 250 GeV. Notice the decrease of missing energy as the neutralino mass increases. Right figure: Restriction in the stop space due the limits on the mass splitting of \tilde{b}_L, \tilde{t}_L , with a lower bound on $m_{\tilde{b}} > 200, 400, 600$ and 800 GeV. The vertical lines correspond to interpreting direct sbottom searches as a $\tilde{t} \rightarrow b\tilde{\chi}^\pm$ decay, leading to the same mass limit.

produce boosted $\chi^{\pm,0}$ unless it itself comes with some boost. For $m_{\tilde{t}} \sim 300$ GeV, this would need some requirement on radiation jets. We illustrate the reduction of missing energy as one increases the value of μ in Fig. 9. Similarly, direct detection of charginos is difficult, due to the degeneracy with the neutralino and small cross sections.

Direct sbottom production searches can be translated into stop production searches when the stop decays to b and χ^\pm , and this search is more encouraging. The ATLAS collaboration performed a search for sbottom squarks, resulting in a 95% C.L. upper limit $m_{\tilde{b}_1} > 390$ GeV for neutralino masses below 60 GeV with $\mathcal{L} = 2.05\text{fb}^{-1}$ [98], but would probably be extended to larger values of m_{χ^0} with the 2012 dataset, being able to cover the case $m_{\tilde{\chi}^{0,\pm}} \lesssim 200$ GeV. Note that direct sbottom searches assume $\text{BR}(\tilde{b} \rightarrow b\tilde{\chi}^0)=1$ but can be re-scaled for lower branching ratios. Moreover, pushing the sbottom limits, within NSUSY, is also an indirect probe of the stop sector due to the custodial relations shown in Sec. IV D. This interplay between direct and indirect limits on stops from direct sbottom production searches is illustrated in Fig. 11, where a maximal mixing case is shown. Interestingly, if the lightest stop is L-dominated, the combination of sbottom and custodial violation limits could be more constraining than the re-interpretation of direct searches in terms of stop decays into charginos. As we do not know the chiral admixture of the stops and sbottoms,

using both strategies would give the best sensitivity. Since sbottom direct detection searches do not suffer many of the problems that affect the advance in collider stop searches, this further supports the observation that direct sbottom searches may be the best direct access to stop parameter space in the near term [60].

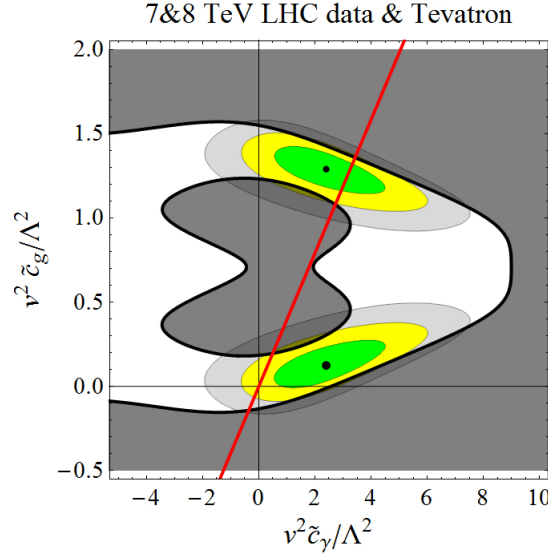


FIG. 10: The region of the higher dimensional operator space excluded at 95% C.L. from current Higgs searches is shown by the black shaded area overlaid on the best-fit regions. The NSUSY relation between the Wilson coefficients is shown with a red line.

Higgs search data also provides a powerful insight into stop parameter space. In particular they offer experimental reach into the large μ region that is such a challenge for collider searches. In Fig. 10, we show the region of the higher dimensional operator space excluded at 95% C.L. from current Higgs searches. Translating this exclusion into the stop parameter space does not lead in general to direct lower mass bound that is independent of δm (when $\theta_{\tilde{t}} \neq 0$) due to the existence of the “funnel region” where a cancelation of the stop contributions to F_g can occur. However, by jointly imposing the condition that the $\text{Br}(\bar{B} \rightarrow X_s \gamma)$ constraint is within its 2σ allowed region, we can define more stringent current exclusion regions for approximately mass degenerate stops. By studying how the Higgs data will scale with more luminosity, we can also project expected exclusions in the stop space by the end of the 8 TeV LHC run. We find the results shown in Fig 11.

In the case of these joint exclusions, there is in general a tail, or spike, of allowed parameter space in the $\text{Br}(\bar{B} \rightarrow X_s \gamma)$ constraint where a significant degree of cancelation is occurring in the NSUSY contributions to $\text{Br}(\bar{B} \rightarrow X_s \gamma)$. This reduces the scaling of this bound in general. This

feature can be seen in Fig. 3 (bottom, right) and the viability of this cancelation region is sensitive to further revisions of the global experimental average of $\text{Br}(\bar{B} \rightarrow X_s \gamma)$ including the recent Babar measurement. If one does not rely on such cancelations to diminish the interplay of the $\text{Br}(\bar{B} \rightarrow X_s \gamma)$ and Higgs search data constraints (outside the funnel region) then the exclusion bounds scale much more quickly, as is also shown in Fig 11.

Note that these exclusions are in the region of $\mu \sim 100 - 200 \text{ GeV}$ in NSUSY and do not require a missing energy tag. This makes indirect studies of stop exclusions from Higgs search data broadly applicable to many SUSY models and these bounds have significant reach into the large μ region. Conversely, collider based searches will be severely challenged to reach the large μ space in direct stop searches due to the fact that the signal region is increasingly similar to the $t\bar{t}$ SM backgrounds with small missing energy.

VII. CONCLUSIONS.

In this paper we have examined the light that Higgs search data sheds on the stop sector of Natural SUSY, where stops are expected to lead to the largest effects on Higgs properties. We have interpreted a generic fit to the latest Higgs data in models which allow for additional BSM contributions to the hgg and $h\gamma\gamma$ couplings in terms of stop parameters. In performing this careful study of the impact of light stop states on Higgs properties, we have included QCD matching corrections and consistently treated the allowed best-fit regions with a one parameter CDF. Further, we have examined in detail the impact of related precision flavour and EW constraints.

Interestingly, we find that a combined global fit to Higgs properties, $\text{Br}(\bar{B} \rightarrow X_s \gamma)$ and Δm_W , show a preference for $\sim 400 - 500 \text{ GeV}$ degenerate stops, that is largely independent of the stop mixing angle. Such a spectrum of stop states cannot explain directly the Higgs mass value of $\sim 125 \text{ GeV}$ but they do offer a good fit to the global dataset we have studied. The quality of fit is comparable to the goodness of fit in the SM. Such a stop spectrum can also improve the agreement of the observed and predicted m_W , ameliorating a very slight tension in the SM with this observable that has arisen with recent precise measurements at the Tevatron. However, we emphasize that what is more interesting at this time is the degree of consistency that the small shift in this precision observable has with the allowed low mass region in the Higgs global fits.

Further, we have also uncovered an exceptional region of parameter space with a light stop eigenstate $m_{\tilde{t}_1} \sim 220 - 260 \text{ GeV}$ and larger mixing, with a second eigenstate that is significantly

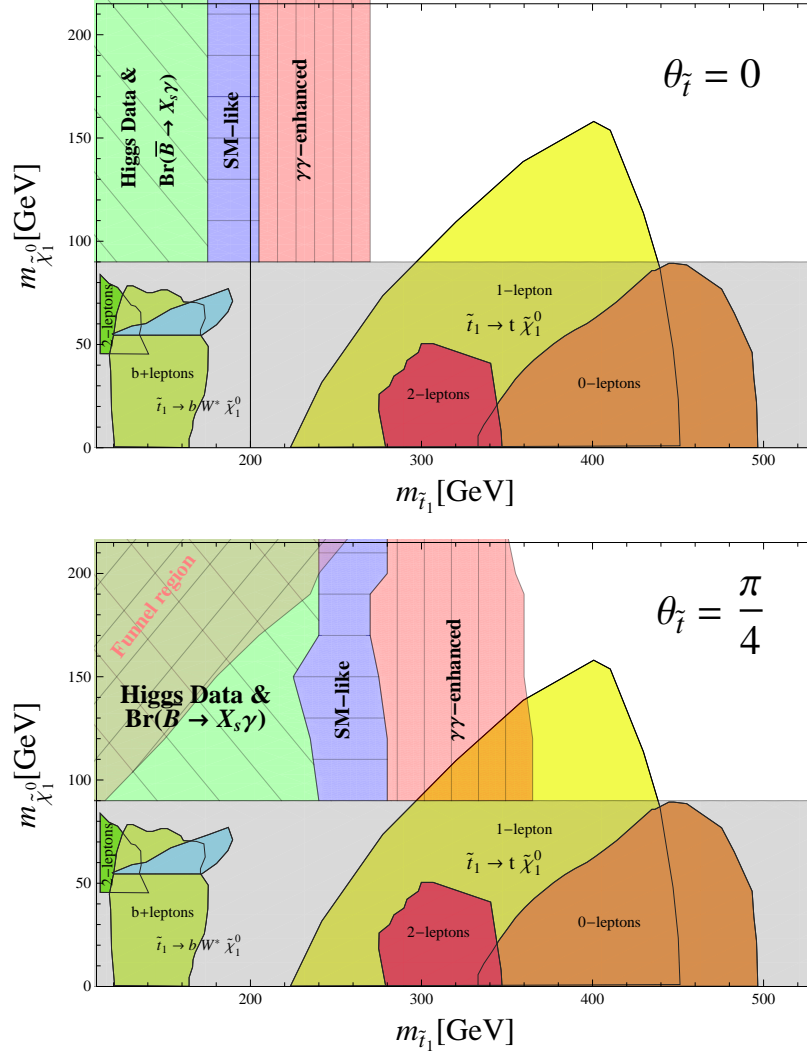


FIG. 11: The current (future) exclusion regions from current (and prospective) Higgs search data that are directly combined with the condition that the $\text{Br}(\bar{B} \rightarrow X_s \gamma)$ constraint is within its 2σ allowed region. Shown are the summary 95% C.L. exclusion results from the dedicated ATLAS collider searches for direct stop production in the $m_{\tilde{t}_1}, \tilde{\chi}_1^0$ plane as solid regions (generally below the line $\tilde{\chi}_1^0 = 90$ GeV). These results are reported in Ref. [67] and were combined into the presented form at ICHEP2012. Added to these figures in the $\tilde{\chi}_1^0 \simeq 90 - 200$ GeV space are current exclusions based on Higgs data and the $\text{Br}(\bar{B} \rightarrow X_s \gamma)$ constraint as a green region with diagonal lines; future exclusions from Higgs search data that evolves to more SM-like values (blue region with horizontal lines, labelled "SM-like") or when the global Higgs data has evolved to have the current 8 TeV central values while its errors have been reduced by a factor of 2 (red region with vertical lines, labelled " $\gamma\gamma$ enhanced"). Top (bottom) figure is the no (maximal) mixing case.

heavier. In this exceptional parameter space region, the presence of such stop states can offer a good global fit to the dataset we have studied of quality comparable or better than the SM and can raise the Higgs mass to its observed value in NSUSY with fine-tuning $\sim 1 - 5\%$ (according to the measure we have adopted). Such stop states can also ameliorate the slight (statistically insignificant) tension in the SM prediction and measurement of m_W . Future careful studies of this form will be essential in ruling out, or confirming a discovery of Natural SUSY at the LHC.

Acknowledgments

We particularly thank M. Mühlleitner for collaboration developing the global fit. We also thank P. Slavich, B. Feigl, R. Harlander, M. Schumacher, M. Spira, W. Fisher, J. Huston, V. Sharma, P. Uwer, J. Bendavid and G. Isidori for helpful communication concerning both theory and data related to the global fit and analysis in this paper. VS would like to thank Xavier Portell for explaining aspects of stop searches at ATLAS. This work has been partly supported by the European Commission under the contract ERC advanced grant 226371 MassTeV, the contract PITN-GA-2009-237920 UNILHC, and the contract MRTN-CT-2006-035863 ForcesUniverse, as well as by the Spanish Consolider Ingenio 2010 Programme CPAN (CSD2007-00042) and the Spanish Ministry MICNN under contract FPA2010-17747 and FPA2008-01430.

Appendix

1. SM Inputs Used

2. Efficiency corrections due to Higher Dimensional Operators

We seek to draw as precise a conclusion as possible about the Higgs signal strength fit to higher dimensional operators with Wilson coefficients $\tilde{c}_g, \tilde{c}_\gamma$ in this paper. The effect of these higher dimensional operators on the signal strength parameters can have two forms. Directly the $\sigma_{gg \rightarrow h}$ and $\Gamma_{h \rightarrow \gamma\gamma}$ rates can be effected, as characterized by our rescaling the data with the effects of $\tilde{c}_g, \tilde{c}_\gamma$ consistently. This effect we fit to directly using our global fit procedure.

There is also a further effect that higher dimensional operators can have on the event yields that lead to the μ_i . The higher dimensional operators can alter the shape of the final kinematic distributions (that sum over more than one production mechanism), leading to a further correction,

Input	Value
m_h	$125 \pm 2 \text{ GeV}$
m_t	$173.2 \pm 0.9 \text{ GeV [99]}$
$m_b(1S)$	$4.65 \pm 0.03 \text{ GeV [100, 101]}$
m_c	$1.275 \pm 0.025 \text{ GeV [101]}$
m_τ	$1776.820.16 \text{ MeV [101]}$
m_Z	$91.1876 \pm 0.0021 \text{ GeV [101]}$
$\alpha_s(M_Z)$	$0.1184 \pm 0.0007 \text{ GeV [102]}$
$(\Delta\alpha)_{had}^{(5)}$	$(275.7 \pm 1) \times 10^{-4} \text{ [103]}$
$(\Delta\alpha)_{lep}$	$(314.97686) \times 10^{-4} \text{ [104]}$
s_W^2	$0.2233 \pm 0.0002 \text{ [101]}$
G_F	$1.1663787 \pm 0.0000006 \times 10^{-5} \text{ GeV}^{-2} \text{ [101]}$

TABLE II: *Input values used in determining constraints on the NSUSY parameters in the indirect tests. When we use the value $\alpha_s(m_t)$ we determine the value from NLO running in QCD finding the central value $\alpha_s(m_t) = 0.1080$.*

as a function of the Wilson coefficient, on the signal strength parameter. The $\tilde{c}_g, \tilde{c}_\gamma$ do not affect the shape of the kinematic distributions due to of an individual production process, such as $gg \rightarrow h \rightarrow \gamma\gamma$, however, they do affect the relative proportions of gg versus Higgstrahlung and VBF initiated Higgs production. This later effect is an “efficiency correction” on the change in the number of expected events expected due to a different effective efficiency for passing the cuts of the experimental analyses when higher dimensional operators are present. This effect is not captured in our direct fit to $\tilde{c}_g, \tilde{c}_\gamma$ and should be quantified for precise conclusions.

We have examined the effect of these efficiency corrections through simulating the effect of those operators in the 7 TeV run data in the $pp \rightarrow h \rightarrow \gamma\gamma (0j, 1j, 2j)$. We added the shift due to the operators in the hgg and $h\gamma\gamma$ effective vertices using Feynrules [105] into an UFO model [106] of MadGraph5 [107]. We generated samples at 7 TeV with a parton level cut on $|\eta_\gamma| < 3.5$ and $p_{T,\gamma} > 20 \text{ GeV}$. The parton level events generated by MadGraph5 are passed to Pythia [108] to simulate the effects of parton showering, and then to Delphes [109] for a fast detector simulation. We use the generic LHC parameters for Delphes, and reconstruct jets with the anti- k_T algorithm using 0.5 for jet cone radius. We cannot simulate all the characteristics of photons in the different

bins, especially the converted/unconverted nature of the photon. Instead, we check the effect of the new physics on the basic selection cuts described in Table III. Those are on top of the detector effects simulated by Delphes, including isolation and energy-momentum smearing.

ATLAS cuts	CMS cuts
$ \eta_{\gamma_{1,2}} < 2.37$	$ \eta_{\gamma_{1,2}} < 2.5$
$p_T^{\gamma_1} > 40 \text{ GeV}, p_T^{\gamma_2} > 25 (30) \text{ GeV}$	$p_T^{\gamma_1} > m_{\gamma\gamma}/3, p_T^{\gamma_2} > m_{\gamma\gamma}/4$
$m_{\gamma\gamma} = 125(126) \pm 3 \text{ GeV}$	$m_{\gamma\gamma} = 125 \pm 3 \text{ GeV}$

TABLE III: Cuts implemented in the Monte Carlo simulation after Delphes. Numbers in parenthesis correspond to the 8 TeV run.

Those cuts are then applied to the signal, containing the SM and the new operators. In Fig. 12 we show the effect of the operators, c_γ, c_g . The effect on the cross section is sizeable, whereas the effect on the efficiencies due to basic p_T, η and $\Delta m_{\gamma\gamma}$ cuts is moderate (less than 1%) except when the cross section drops due to a cancellation between the SM and new physics contributions.

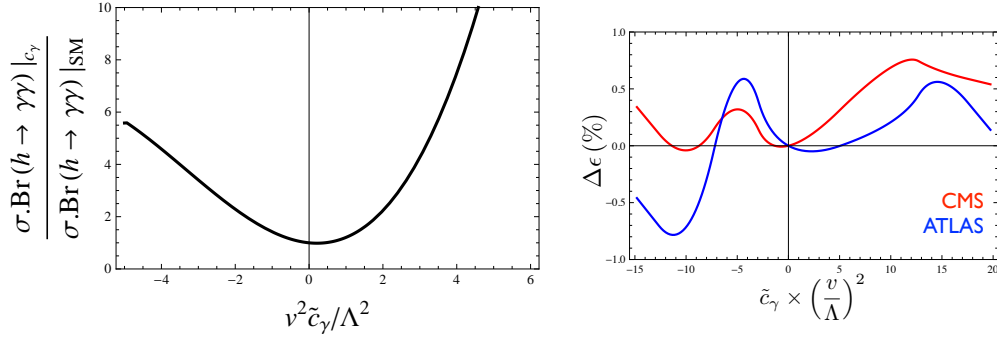


FIG. 12: Left: The cross section as a function of c_γ, c_g using the fixed relationship between the Wilson coefficients. Right: Change in efficiencies to the cuts defined in Table. III. Both figures correspond to $\sqrt{s} = 7 \text{ TeV}$.

The effect on efficiencies for the relation between c_γ and c_g given in Eq. 20 is very similar to Fig. 12, namely of the order $\lesssim 1 \%$. Further the corrections stay at this level when both operators are present or when the effects at 8 TeV are simulated as we have explicitly verified. Due to this small correction we neglect effects due to efficiency corrections due to higher dimensional operators in this paper.

3. $\text{Br}(\bar{B} \rightarrow X_s \gamma)$ Loop Functions

The loop functions in $\text{Br}(\bar{B} \rightarrow X_s \gamma)$ are given by [45, 54, 110]

$$F_7^1(x) = \frac{x(7 - 5x - 8x^2)}{24(x - 1)^3} + \frac{x^2(3x - 2)}{4(x - 1)^4} \log x, \quad (\text{A.1})$$

$$F_8^1(x) = \frac{x(2 + 5x - x^2)}{8(x - 1)^3} + \frac{3x^2}{4(x - 1)^4} \log x, \quad (\text{A.2})$$

$$F_7^3(x) = \frac{5 - 7x}{6(x - 1)^2} + \frac{x(3x - 2)}{3(x - 1)^3} \log x, \quad (\text{A.3})$$

$$F_8^3(x) = \frac{1 + x}{2(x - 1)^2} - \frac{x}{(x - 1)^3} \log x. \quad (\text{A.4})$$

- [1] S. Dimopoulos and G. F. Giudice, Phys. Lett. B **357**, 573 (1995) [hep-ph/9507282].
- [2] A. Pomarol and D. Tommasini, Nucl. Phys. B **466** (1996) 3 [hep-ph/9507462].
- [3] A. G. Cohen, D. B. Kaplan and A. E. Nelson, Phys. Lett. B **388**, 588 (1996) [hep-ph/9607394].
- [4] R. Kitano and Y. Nomura, Phys. Rev. D **73** (2006) 095004 [hep-ph/0602096].
- [5] Y. Kats, P. Meade, M. Reece and D. Shih, JHEP **1202**, 115 (2012) [hep-ph/1110.6444].
- [6] C. Brust, A. Katz, S. Lawrence and R. Sundrum, [hep-ph/1110.6670]. C. Brust, A. Katz and R. Sundrum, [hep-ph/1206.2353].
- [7] M. Papucci, J. T. Ruderman and A. Weiler, [hep-ph/1110.6926].
- [8] M. Carena, S. Gori, N. R. Shah, C. E. M. Wagner and L. -T. Wang, [hep-ph/1205.5842].
- [9] K. Blum, R. T. D’Agnolo and J. Fan, [hep-ph/1206.5303].
- [10] D. Carmi, A. Falkowski, E. Kuflik and T. Volansky, [hep-ph/1202.3144].
- [11] D. Carmi, A. Falkowski, E. Kuflik, T. Volansky, J Zupan [hep-ph/1207.1718].
- [12] M. Carena, S. Gori, N. R. Shah and C. E. M. Wagner, JHEP **1203**, 014 (2012) [hep-ph/1112.3336].
- [13] T. Cohen, D. E. Morrissey and A. Pierce, [hep-ph/1203.2924].
- [14] A. Arvanitaki and G. Villadoro, JHEP **1202**, 144 (2012) [hep-ph/1112.4835].
- [15] A. Arbey, *et al.* Phys. Lett. B **708**, 162 (2012) [hep-ph/1112.3028].
- [16] D. Curtin, P. Jaiswal and P. Meade, [hep-ph/1203.2932].
- [17] A. Azatov, S. Chang, N. Craig and J. Galloway, [hep-ph/1206.1058].
- [18] See ATLAS & CMS’s summary of the searches. <https://twiki.cern.ch/twiki/bin/view/AtlasPublic/SupersymmetryPublicResults>, <https://twiki.cern.ch/>

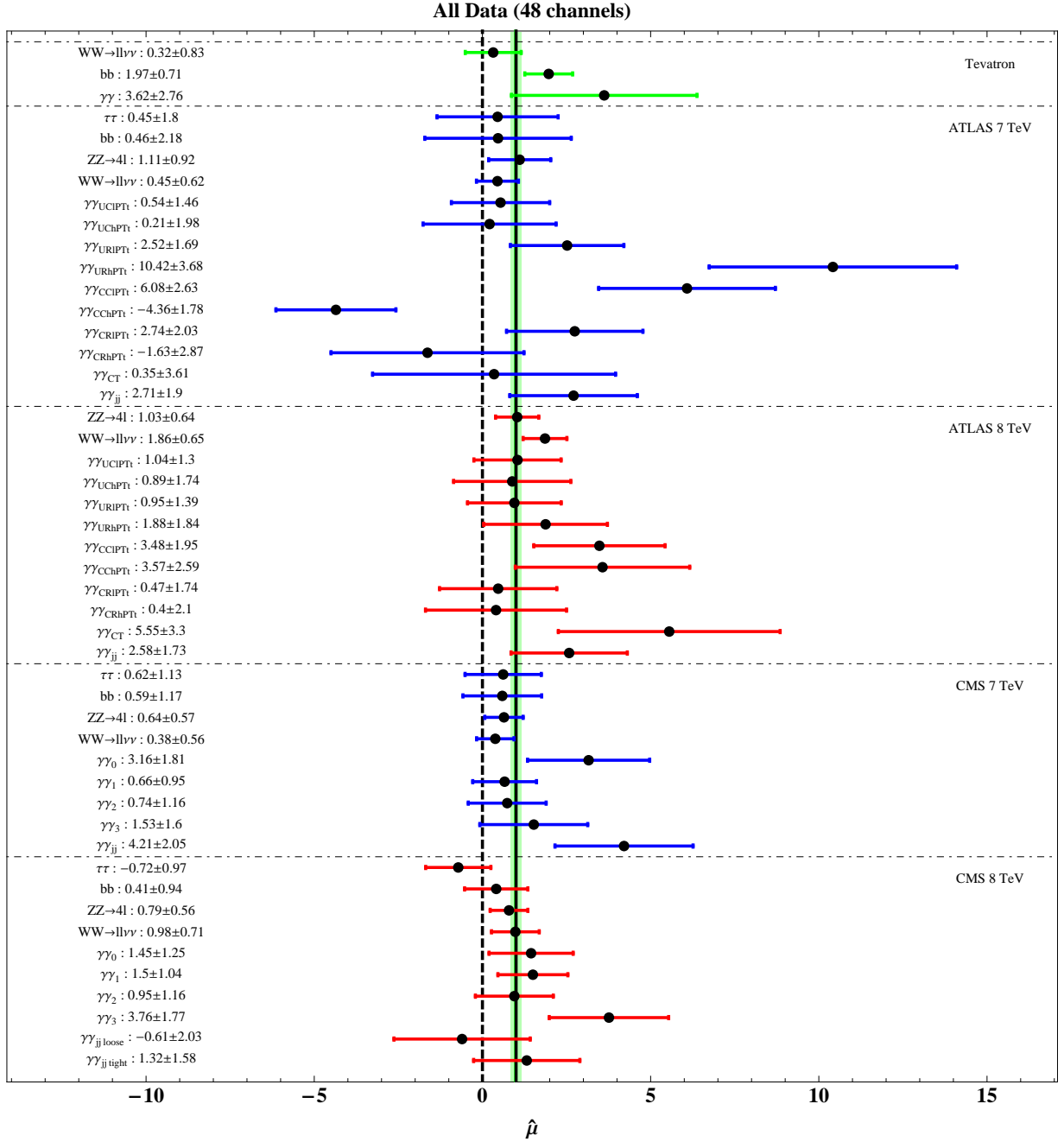


FIG. 13: Summary of Higgs best-fit signal-strengths $\hat{\mu}_i$ used in our global fit. For more details see Ref. [26–28]. Shown are the reported $\hat{\mu}_i$ (or the reconstructed 8 TeV value if not directly reported [28]). For CMS and the Tevatron we use values at $m_h = 125$ GeV, while for ATLAS we use $m_h = 126.5$ GeV. This choice is partially due to the limited experimental information currently supplied. For discussions on possible bias from this choice see Ref. [28, 111]. Also shown is the combined $\hat{\mu}$ and error as a vertical green band and the SM expected signal strength as a black vertical line at $\hat{\mu} = 1$.

twiki/bin/view/CMSPublic/PhysicsResultsSUS.

- [19] J. R. Ellis, M. K. Gaillard and D. V. Nanopoulos, Nucl. Phys. B **106**, 292 (1976).
- [20] A. Djouadi, Phys. Lett. B **435**, 101 (1998) [hep-ph/9806315].
- [21] A. Djouadi, *et al.* Eur. Phys. J. C **1**, 149 (1998) [hep-ph/9612362].
- [22] A. V. Manohar and M. B. Wise, Phys. Lett. B **636**, 107 (2006) [hep-ph/0601212].
- [23] S. Dawson, A. Djouadi and M. Spira, Phys. Rev. Lett. **77**, 16 (1996) [hep-ph/9603423].
- [24] R. V. Harlander and M. Steinhauser, Phys. Lett. B **574**, 258 (2003) [hep-ph/0307346].
- [25] R. V. Harlander and M. Steinhauser, JHEP **0409**, 066 (2004) [hep-ph/0409010].
- [26] J. R. Espinosa, C. Grojean, M. Muhlleitner and M. Trott, JHEP **1205**, 097 (2012) [hep-ph/1202.3697].
- [27] J. R. Espinosa, C. Grojean, M. Muhlleitner and M. Trott, [hep-ph/1205.6790].
- [28] J. R. Espinosa, C. Grojean, M. Muhlleitner and M. Trott, [hep-ph/1207.1717].
- [29] P. P. Giardino *et al.* [hep-ph/1207.1347].
- [30] J. Ellis and T. You, JHEP **1206**, 140 (2012) [hep-ph/1204.0464]; [hep-ph/1207.1693].
- [31] R. Lafaye *et al.* JHEP **0908**, 009 (2009) [hep-ph/0904.3866].
- [32] C. Englert *et al.* Phys. Lett. B **707**, 512 (2012) [hep-ph/1112.3007].
- [33] M. Klute *et al.* [hep-ph/1205.2699].
- [34] T. Corbett, O. J. P. Eboli, J. Gonzalez-Fraile and M. C. Gonzalez-Garcia, [hep-ph/1207.1344].
- [35] A. Azatov, R. Contino and J. Galloway, [hep-ph/1206.3171].
- [36] ATLAS and CMS collaborations, Wed July 4th, CERN.
- [37] LPCC meeting, Friday, July 13, 2012 <https://indico.cern.ch/getFile.py/access?contribId=1&sessionId=0&resId=1&materialId=slides&confId=173388>
- [38] G. Aad *et al.* [ATLAS Collaboration], [hep-ex/1207.0319].
- [39] S. Chatrchyan *et al.* [CMS Collaboration], Phys. Lett. B **710**, 26 (2012) [hep-ex/1202.1488].
- [40] Tevatron New Pheno. Higgs WG, http://tevnpnphwg.fnal.gov/results/SM_Higgs_Summer_12/index.html
- [41] S. Dittmaier *et al.* [LHC Higgs Cross Section WGC], [hep-ph/1101.0593].
- [42] F. Bonnet, T. Ota, M. Rauch and W. Winter, arXiv:1207.4599 [hep-ph].
- [43] S. Ferrara and E. Remiddi, Phys. Lett. B **53**, 347 (1974).
- [44] B. Grinstein, R. P. Springer and M. B. Wise, Phys. Lett. B **202**, 138 (1988).
- [45] S. Bertolini, F. Borzumati, A. Masiero and G. Ridolfi, Nucl. Phys. B **353**, 591 (1991).

- [46] S. Eidelman *et al.* [Particle Data Group Collaboration], Phys. Lett. B **592**, 1 (2004).
- [47] A. E. Nelson, N. Rius, V. Sanz and M. Unsal, JHEP **0208**, 039 (2002) [hep-ph/0206102].
- [48] G. D. Kribs, E. Poppitz and N. Weiner, Phys. Rev. D **78**, 055010 (2008) [hep-ph/0712.2039].
- [49] R. S. Chivukula and H. Georgi, Phys. Lett. B **188** (1987) 99.
- [50] L. J. Hall and L. Randall, Phys. Rev. Lett. **65**, 2939 (1990).
- [51] G. D'Ambrosio, G. F. Giudice, G. Isidori and A. Strumia, Nucl. Phys. B **645** (2002) 155 [hep-ph/0207036].
- [52] A. J. Buras, Acta Phys. Polon. B **34**, 5615 (2003) [hep-ph/0310208].
- [53] V. Cirigliano, B. Grinstein, G. Isidori and M. B. Wise, Nucl. Phys. B **728** (2005) 121 [hep-ph/0507001].
- [54] B. Grzadkowski and M. Misiak, Phys. Rev. D **78**, 077501 (2008) [hep-ph/0802.1413].
- [55] D. Asner *et al.* [Heavy Flavor Averaging Group Collaboration], [hep-ex/1010.1589].
- [56] [The BABAR Collaboration], [hep-ex/1207.5772].
- [57] T. Aaltonen *et al.* [CDF], Phys. Rev. Lett. **108**, 151803 (2012) [hep-ex/1203.0275].
- [58] V. M. Abazov *et al.* [D0], Phys. Rev. Lett. **108**, 151804 (2012) [hep-ex/1203.0293].
- [59] Tevatron EW Group, f. t. C. Collaboration and D. Collaboration, [hep-ex/1204.0042].
- [60] H. M. Lee, V. Sanz and M. Trott, JHEP **1205**, 139 (2012) [hep-ph/1204.0802].
- [61] V. Barger, P. Huang, M. Ishida and W. -Y. Keung, [hep-ph/1206.1777].
- [62] M. Awramik, *et al.* Phys. Rev. D **69**, 053006 (2004) [hep-ph/0311148].
- [63] R. Barbieri and L. Maiani, Nucl. Phys. B **224** (1983) 32.
- [64] M. Drees and K. Hagiwara, Phys. Rev. D **42**, 1709 (1990).
- [65] P. H. Chankowski *et al.* Nucl. Phys. B **417**, 101 (1994).
- [66] S. Heinemeyer *et al.* JHEP **0608**, 052 (2006) [hep-ph/0604147].
- [67] ATLAS-CONF-2012-036. ATLAS-CONF-2012-074. ATLAS-CONF-2012-073.
ATLAS-CONF-2012-071. ATLAS-CONF-2012-070. ATLAS-CONF-2012-059.
- [68] Y. Bai, H. -C. Cheng, J. Gallicchio and J. Gu, [hep-ph/1203.4813].
- [69] Z. Han, A. Katz, D. Krohn and M. Reece, [hep-ph/1205.5808].
- [70] D. S. M. Alves, M. R. Buckley, P. J. Fox, J. D. Lykken and C. -T. Yu, [hep-ph/1205.5805].
- [71] D. E. Kaplan, K. Rehermann and D. Stolarski, [hep-ph/1205.5816].
- [72] CMS, S. Chatrchyan *et al.*, [hep-ex/1204.0821].
- [73] ATLAS-CONF-2012-085.

- [74] G. Belanger, M. Heikinheimo and V. Sanz, [hep-ph/1205.1463].
- [75] H. K. Dreiner and M. K. J. Tattersall, [hep-ph/1207.1613].
- [76] G. Aad *et al.* [ATLAS Collaboration], Phys. Lett. B **710**, 67 (2012) [hep-ex/1109.6572]. ATLAS-CONF-2012-033.ATLAS-CONF-2012-041.
- [77] CMS-SUS-12-011-003. See CMS SUSY webpage for more information.
- [78] PAS-SUS-11-016, see CMS SUSY webpage.
- [79] PAS-SUS-12-016, see CMS SUSY webpage.
- [80] M. Heikinheimo, M. Kellerstein and V. Sanz, JHEP **1204**, 043 (2012) [hep-ph/1111.4322].
- [81] Y. Okada, M. Yamaguchi and T. Yanagida, Prog. Theor. Phys. **85**, 1 (1991); J. R. Ellis, G. Ridolfi and F. Zwirner, Phys. Lett. B **257**, 83 (1991); H. E. Haber and R. Hempfling, Phys. Rev. Lett. **66**, 1815 (1991).
- [82] G. Degrassi, S. Heinemeyer, W. Hollik, P. Slavich and G. Weiglein, Eur. Phys. J. C **28** (2003) 133 [hep-ph/0212020].
- [83] S. Heinemeyer, W. Hollik and G. Weiglein, Comput. Phys. Commun. **124** (2000) 76 [hep-ph/9812320].
- [84] A. Djouadi *et al.* Comput. Phys. Commun. **176** (2007) 426 [hep-ph/0211331].
- [85] M. S. Carena, J. R. Espinosa, M. Quiros and C. E. M. Wagner, Phys. Lett. B **355** (1995) 209 [hep-ph/9504316]; S. Heinemeyer, W. Hollik and G. Weiglein, Phys. Lett. B **455** (1999) 179 [hep-ph/9903404]; J. R. Espinosa and R. -J. Zhang, JHEP **0003** (2000) 026 [hep-ph/9912236]; M. S. Carena, H. E. Haber, S. Heinemeyer, W. Hollik, C. E. M. Wagner and G. Weiglein, Nucl. Phys. B **580** (2000) 29 [hep-ph/0001002]; J. R. Espinosa and R. -J. Zhang, Nucl. Phys. B **586** (2000) 3 [hep-ph/0003246]; G. Degrassi, P. Slavich and F. Zwirner, Nucl. Phys. B **611** (2001) 403 [hep-ph/0105096]; A. Brignole, G. Degrassi, P. Slavich and F. Zwirner, Nucl. Phys. B **631** (2002) 195 [hep-ph/0112177].
- [86] J. R. Espinosa and I. Navarro, Nucl. Phys. B **615** (2001) 82 [hep-ph/0104047].
- [87] M. Drees, Int. J. Mod. Phys. A **4** (1989) 3635; J. R. Ellis, J. F. Gunion, H. E. Haber, L. Roszkowski and F. Zwirner, Phys. Rev. D **39** (1989) 844; P. Binetruy and C. A. Savoy, Phys. Lett. B **277** (1992) 453; J. R. Espinosa and M. Quiros, Phys. Lett. B **279** (1992) 92; Phys. Rev. Lett. **81** (1998) 516 [hep-ph/9804235]; G. L. Kane, C. F. Kolda and J. D. Wells, Phys. Rev. Lett. **70** (1993) 2686 [hep-ph/9210242]; M. Masip, R. Munoz-Tapia and A. Pomarol, Phys. Rev. D **57** (1998) R5340 [hep-ph/9801437]; M. Bastero-Gil, C. Hugonie, S. F. King, D. P. Roy and S. Vempati, Phys. Lett. B **489**

- (2000) 359 [hep-ph/0006198].
- [88] D. Comelli and C. Verzegnassi, Phys. Lett. B **303** (1993) 277; J. R. Espinosa and M. Quiros, Phys. Lett. B **302** (1993) 51 [hep-ph/9212305]; P. Batra, A. Delgado, D. E. Kaplan and T. M. P. Tait, JHEP **0402** (2004) 043 [hep-ph/0309149].
- [89] N. Polonsky and S. Su, Phys. Lett. B **508** (2001) 103 [hep-ph/0010113]; A. Strumia, Phys. Lett. B **466** (1999) 107 [hep-ph/9906266]; A. Brignole, J. A. Casas, J. R. Espinosa and I. Navarro, Nucl. Phys. B **666** (2003) 105 [hep-ph/0301121]; J. A. Casas, J. R. Espinosa and I. Hidalgo, JHEP **0401** (2004) 008 [hep-ph/0310137]; M. Dine, N. Seiberg and S. Thomas, Phys. Rev. D **76** (2007) 095004 [hep-ph/0707.0005].
- [90] J. R. Ellis, K. Enqvist, D. V. Nanopoulos and F. Zwirner, Mod. Phys. Lett. A **1**, 57 (1986).
- [91] R. Barbieri and G. F. Giudice, Nucl. Phys. B **306**, 63 (1988).
- [92] M. Perelstein and C. Spethmann, JHEP **0704**, 070 (2007) [hep-ph/0702038].
- [93] L. J. Hall, D. Pinner and J. T. Ruderman, JHEP **1204** (2012) 131 [hep-ph/1112.2703].
- [94] [ATLAS Collaboration], [hep-ex/1112.3832].
- [95] H. Li, W. Parker, Z. Si and S. Su, Eur. Phys. J. C **71**, 1584 (2011) [hep-ph/1009.6042].
- [96] A. Datta and S. Niyogi, [hep-ph/1111.0200].
- [97] E. Alvarez and Y. Bai, [hep-ph/1204.5182].
- [98] G. Aad *et al.* [ATLAS], Phys. Rev. Lett. **108**, 181802 (2012) [hep-ex/1112.3832].
- [99] [Tevatron EW Group], [hep-ex/1107.5255].
- [100] C. W. Bauer, Z. Ligeti, M. Luke, A. V. Manohar and M. Trott, Phys. Rev. D **70**, 094017 (2004) [hep-ph/0408002].
- [101] K. Nakamura *et al.* [Particle Data Group Collaboration], J. Phys. G G **37**, 075021 (2010).
- [102] S. Bethke, Eur. Phys. J. C **64**, 689 (2009) [hep-ph/0908.1135].
- [103] M. Davier, A. Hoecker, B. Malaescu and Z. Zhang, Eur. Phys. J. C **71**, 1515 (2011) [Erratum-ibid. C **72**, 1874 (2012)] [hep-ph/1010.4180].
- [104] M. Steinhauser, Phys. Lett. B **429**, 158 (1998) [hep-ph/9803313].
- [105] N. D. Christensen and C. Duhr, Comput. Phys. Commun. **180**, 1614 (2009) [hep-ph/0806.4194].
- [106] C. Degrande *et al.* Comput. Phys. Commun. **183**, 1201 (2012) [hep-ph/1108.2040].
- [107] J. Alwall *et al.* JHEP **1106**, 128 (2011) [hep-ph/1106.0522].
- [108] T. Sjostrand, S. Mrenna and P. Z. Skands, JHEP **0605**, 026 (2006) [hep-ph/0603175].
- [109] S. Ovnyn, X. Roubey and V. Lemaitre, [hep-ph/0903.2225].

- [110] G. Degrassi, P. Gambino and G. F. Giudice, JHEP **0012**, 009 (2000) [hep-ph/0009337].
- [111] B. Murray, RAL Higgs Workshop 28th March 2012, <http://indico.cern.ch/getFile.py/access?contribId=84&sessionId=18&resId=0&materialId=slides&confId=162621>